ISTANBUL TECHNICAL UNIVERSITY ★ GRADUATE SCHOOL

SUPPRESSION OF SYMMETRY-BREAKING BIFURCATIONS OF OPTICAL SOLITONS IN PARITY-TIME SYMMETRIC POTENTIALS

M.Sc. THESIS

Melis TURGUT

Department of Mathematics Engineering

Mathematics Engineering Programme

DECEMBER 2022

ISTANBUL TECHNICAL UNIVERSITY ★ GRADUATE SCHOOL

SUPPRESSION OF SYMMETRY-BREAKING BIFURCATIONS OF OPTICAL SOLITONS IN PARITY-TIME SYMMETRIC POTENTIALS

M.Sc. THESIS

Melis TURGUT
(509181205)

Department of Mathematics Engineering

Mathematics Engineering Programme

Thesis Advisor: Prof. Dr. İlkay BAKIRTAŞ AKAR

DECEMBER 2022

İSTANBUL TEKNİK ÜNİVERSİTESİ ★ LİSANSÜSTÜ EĞİTİM ENSTİTÜSÜ

PARİTE-ZAMAN SİMETRİSİNE SAHİP POTANSİYELLERDE OPTİK SOLİTONLARIN SİMETRİ KIRILMASI ÇATALLANMASININ BASKILANMASI

YÜKSEK LİSANS TEZİ

Melis TURGUT
(509181205)

Matematik Mühendisliği Anabilim Dalı

Matematik Mühendisliği Programı

Tez Danışmanı: Prof. Dr. İlkay BAKIRTAŞ AKAR

ARALIK 2022

Melis TURGUT, a M.Sc. student of ITU Graduate School student ID 509181205, successfully defended the thesis entitled "SUPPRESSION OF SYMMETRY-BREAKING BIFURCATIONS OF OPTICAL SOLITONS IN PARITY-TIME SYMMETRIC POTENTIALS", which she prepared after fulfilling the requirements specified in the associated legislations, before the jury whose signatures are below.

Thesis Advisor :	**Prof. Dr. İlkay BAKIRTAŞ AKAR** Istanbul Technical University	.....
Jury Members :	**Prof. Dr. Nalan ANTAR** Istanbul Technical University	.....
	Assoc. Prof. Dr. Mahmut BAĞCI Marmara University	.....

Date of Submission : 17 November 2022
Date of Defense : 9 December 2022

To my family,

FOREWORD

First and foremost, I would like to express my deepest gratitude to my advisor Prof. Dr. İlkay Bakırtaş for her patience, encouragement, and immense knowledge during my studies. I have overcome all difficulties thanks to her belief in me and moral support. She will always be my role model with her inspiring creativity and wisdom.

Besides, I wish to thank Prof. Dr. Nalan Antar, who always supported me with her instructive comments and valuable contributions when I needed help. I would also like to thank my colleague Eril Güray Çelik, with whom we are in the same working group, for all his help and collaboration.

Last but not least, I would like to thank my dearest family for their unconditional love and unwavering support throughout my life.

December 2022 Melis TURGUT

TABLE OF CONTENTS

Page

ABBREVIATIONS

NLS	**:** Nonlinear Schrödinger
GVD	**:** Second Order (Group-Velocity) Dispersion
TOD	**:** Third Order Dispersion
FOD	**:** Fourth Order Dispersion
CQNLS	**:** Cubic-Quintic Nonlinear Schrödinger
(1+1)D	**:** One Plus One Dimensional
KdV	**:** Korteweg-de Vries
SOM	**:** Squared-Operator Method
$\mathcal{PT}$	**:** Parity-Time
Eq.	**:** Equation
Eqs.	**:** Equations

LIST OF FIGURES

Page

SUPPRESSION OF SYMMETRY-BREAKING BIFURCATIONS OF OPTICAL SOLITONS IN PARITY-TIME SYMMETRIC POTENTIALS

SUMMARY

Optical soliton refers to any optical field that maintains its special structure during propagation because of the balance between diffraction and self-phase modulation of the medium. The dynamics of optical solitons are investigated comprehensively due to their fundamental structures and potential applications. In particular, optical solitons play an important role in fiber optic communication system that uses pulses of infrared light to transmit information from one place to another over a long distance.

The propagation of the electromagnetic wave in optical fibers is modeled by the cubic-quintic nonlinear Schrödinger (CQNLS) equation

$$i\Psi_z + \Psi_{xx} + \alpha |\Psi|^2 \Psi + \beta |\Psi|^4 \Psi = 0, \tag{1}$$

where $\Psi(x,z)$ is normalized complex-valued slowly varying pulse envelope of the electric field, z is the scaled propagation distance, x is the transverse coordinate, Ψ_{xx} corresponds to diffraction, α and β are the coefficients of cubic and quintic nonlinearities, respectively.

A higher-order dispersion needs to be considered for performance enhancement along trans-oceanic and trans-continental distances. Fourth order dispersion needs to be taken into account for short pulse widths where the group velocity dispersion changes within the spectral bandwidth of the signal. In addition, it is known from many studies in the literature that an external potential added to the system can be also beneficial for performance improvement.

In this thesis, we consider the nonlinear paraxial beam propagation in cubic-quintic nonlinearity with a complex parity-time ($\mathcal{PT}$) symmetric potential and fourth order dispersion. This propagation is modeled by the following CQNLS equation

$$i\Psi_z + \Psi_{xx} - \gamma \Psi_{xxxx} + V(x)\Psi + \alpha |\Psi|^2 \Psi + \beta |\Psi|^4 \Psi = 0, \tag{2}$$

where $\gamma > 0$ is the coupling constant of the fourth order dispersion, $V(x)$ represents a complex $\mathcal{PT}$-symmetric potential. In this thesis, we consider $\mathcal{PT}$-symmetric potentials that are of the form

$$V(x) = g^2(x) + c_0 g(x) + ig'(x), \tag{3}$$

where $g(x)$ is an arbitrary real and even function, c_0 is an arbitrary real constant and $\mathcal{PT}$-symmetric solitons undergo symmetry breaking. We take a localized double-hump function $g(x)$ in the form of

$$g(x) = A\left(e^{-(x+x_0)^2} + e^{-(x-x_0)^2}\right), \tag{4}$$

where A and x_0 are related to the modulation strength and separation of $\mathcal{PT}$-symmetric potential, respectively.

The soliton solutions of CQNLS equation with fourth order dispersion and a complex $\mathcal{PT}$-symmetric potential are numerically obtained by means of the squared-operator method since the equation is nonintegrable. The linear stability analysis of the numerically obtained solitons is examined by linear spectrum analysis and the nonlinear stability analysis is examined by nonlinear evolution with split-step Fourier method.

The existence of symmetry breaking of solitons and suppression of symmetry-breaking bifurcations have been investigated. To examine the effect of fourth order dispersion on this symmetry breaking, the coefficient of fourth order dispersion γ is incremented gradually. Consequently, we have demonstrated that the symmetry-breaking bifurcation of the solitons in this problem is completely suppressed as the strength of the fourth order dispersion increases. Moreover, increasing the strength of fourth order dispersion positively influences the linear and nonlinear stability behaviors of solitons.

PARİTE-ZAMAN SİMETRİSİNE SAHİP POTANSİYELLERDE OPTİK SOLİTONLARIN SİMETRİ KIRILMASI ÇATALLANMASININ BASKILANMASI

ÖZET

Doğadaki birçok olay, doğrusal olmayan kısmi türevli diferansiyel denklemler kullanılarak matematiksel olarak modellenmektedir. Geniş bir doğrusal olmayan dispersif kısmi türevli diferansiyel denklemler sınıfı, doğrusal olmayan dalga yayılım problemlerinde önemli bir rol oynayan ilerleyen dalga çözümlerine sahiptirler. Sıklıkla, doğrusal olmayan dalga yayılımı problemleri, doğrusal olmayan optik, Bose-Einstein yoğunlaşmaları, akışkanlar dinamiği, plazma fiziği, elastik ortamlar ve biyoloji gibi çeşitli alanlarda gözlemlenir. Bir tekil dalga veya soliton, sabit hızda herhangi bir bozulma olmadan yayılabilen bir dalga paketi veya bir darbe şeklinde olan özel bir lokalize ilerleyen dalga çözümüdür.

Doğrusal olmayan optikte, solitonlar, ortamın grup hız dispersiyonu ve kendi kendine faz modülasyonu arasındaki denge nedeniyle yayılma sırasında şekilleri değişmeden ilerleyebilirler. Optik solitonlar temel yapıları ve bu özellikleri sonucunda potansiyel uygulamaları nedeniyle son yıllarda en heyecan verici araştırma alanlarından biri olmuştur. Özellikle, elektronik sinyalleri ışığa dönüştürerek uzun mesafede verileri bir fiber üzerinden iletmek için ışık dalgası teknolojisini kullanan fiber optik haberleşme sistemlerinde önemli bir yere sahiptirler.

Elektromanyetik dalganın fiber optik kablolarda yayılımı aşağıda verilen kübik-kuintik doğrusal olmayan Schrödinger (CQNLS) denklemi ile modellenir:

$$i\Psi_z + \Psi_{xx} + \alpha |\Psi|^2 \Psi + \beta |\Psi|^4 \Psi = 0. \quad \textbf{(5)}$$

Bu denklemde Ψ türevlenebilir kompleks değerli fonksiyonu, elektrik alanının yavaş değişen genliğini, Ψ_{xx} difraksiyonu (kırınımı), z yayılım uzaklığını, α ve β, sırasıyla, kübik ve kuintik doğrusal olmayanlık katsayılarını temsil etmektedir. Difraksiyonun su dalgalarındaki karşılığı dispersiyondur.

Ultra kısa atımlar çalışılırken sadece ikinci mertebeden dispersiyonun değil, üçüncü ve dördüncü mertebeden dispersiyonun da modele eklenmeleri gerektiği fark edilmiştir. Okyanus ötesi ve kıtalar arası mesafelerde performans artışı için daha yüksek dereceli dispersiyonun dikkate alınması gerekir. Ayrıca, grup hız dağılımının sinyalin spektral bant genişliği içinde değiştiği kısa atım genişlikleri için dördüncü mertebeden dispersiyon (FOD) modele eklenmelidir. Ek olarak, literatürdeki birçok çalışma sayesinde sisteme eklenen bir dış potansiyelin de performans artırımı için yararlı olabileceği bilinmektedir.

Bu tezde, yukarıda bahsedilen özellikler düşünülerek dördüncü mertebeden dispersiyon ve kompleks bir dış potansiyel içeren CQNLS denklemi ele alınmıştır:

$$i\Psi_z + \Psi_{xx} - \gamma\,\Psi_{xxxx} + V(x)\Psi + \alpha\,|\Psi|^2\,\Psi + \beta\,|\Psi|^4\,\Psi = 0. \tag{6}$$

Burada $\gamma > 0$ dördüncü mertebeden dispersiyonun katsayısını, $V(x) = V_{re}(x) + iV_{im}(x)$ kompleks değerli bir dış potansiyeli temsil etmektedir.

Optik dalga kılavuzu enerji kazancı ve kaybı içeriyorsa, ortamın optik potansiyeli karmaşık değerli olacaktır. Bu çalışmada, aşağıda verilen parite-zaman ($\mathcal{PT}$) simetrisine sahip dış potansiyel alınmıştır:

$$V(x) = g^2(x) + c_0 g(x) + ig'(x), \tag{7}$$

$g(x)$ gerçel değerli keyfi bir çift fonksiyondur, c_0 ise gerçel değerli keyfi bir sabittir. Genel olarak $\mathcal{PT}$-simetrik potansiyellerde, $\mathcal{PT}$-simetrik solitonlar simetri kırılmasına maruz kalmazlar. Ancak bu özel potansiyel için solitonların $\mathcal{PT}$-simetrisi bozulabilir. Buradaki $g(x)$ fonksiyonu çift-tümsekli lokalize bir formda alınmıştır:

$$g(x) = A\left(e^{-(x+x_0)^2} + e^{-(x-x_0)^2}\right), \tag{8}$$

A fonksiyonun maksimum genliğini ve x_0 tümseklerin yerel maksimumlarının konumlarının x koordinatlarını belirlemektedir.

Bilim ve mühendislik alanlarındaki birçok doğrusal olmayan dalga yayılımı problemleri integrallenemeyen denklemlerle yönetilir. Yukarıda verilen dördüncü mertebeden dispersiyon ve bir dış potansiyel içeren CQNLS denklemi de integrallenemez olduğu için analitik olarak çözmek mümkün değildir. Bu nedenle, ilgili CQNLS denkleminin soliton çözümlerinin varlığını ve dinamiklerini incelemek için sayısal yöntemler gereklidir.

Birinci bölümde, tezde ele alınan problem ile ilgili kavramlar parçalara ayrılarak gerekli bilgiler verilmiştir. NLS-tipi denklemlerin yapısı temelden başlanıp, kullanım alanlarına göre gerekli bilgiler eklenerek tezde incelenecek olan problemin özellikleri ve tezin amacı açıklanmıştır. Daha sonra solitonların tarihsel gelişiminden kısaca bahsedilip, ilgili literatür taraması verilmiştir.

İkinci bölümde, bu çalışmada kullanılan sayısal yöntemler yer almaktadır. İlk olarak, kare-operatör yöntemi dördüncü mertebeden dispersiyon ve $\mathcal{PT}$-simetrik potansiyel içeren CQNLS denkleminin soliton çözümlerini bulmak amacıyla, $\Psi(x,z) = \psi(x)e^{i\mu z}$ çözüm önerisi kullanılarak geliştirilmiştir. Burada, $\psi(x)$ kompleks değerli lokalize bir fonksiyondur ve μ gerçel değerli yayılım sabitini temsil etmektedir. Daha sonra Fourier kollokasyon yönteminin uygulanışı genel tipte doğrusal olmayanlık içeren NLS denklemi üzerinden anlatılmıştır.

Üçüncü bölümde, sayısal olarak elde edilen soliton çözümlerinin doğrusal ve doğrusal olmayan kararlılık analizini yapabilmek için, sırasıyla, dördüncü mertebeden dispersiyon ve $\mathcal{PT}$-simetrik potansiyel içeren CQNLS denklemine karşılık gelen doğrusallaştırılmış operatörün doğrusal spektrumunu veren özdeğer problemi ve ayrık-adımlı Fourier yönteminin bu CQNLS denklemine uygulanışı verilmiştir.

Dördüncü bölümde, dördüncü mertebeden dispersiyon ve $\mathcal{PT}$-simetrik potansiyel içeren CQNLS denkleminin soliton çözümlerinin ve simetri kırılmasının varlığı

incelenmiştir. Bu amaçla, dördüncü mertebeden dispersiyon katsayısı γ kademeli olarak arttırılmıştır. Dördüncü mertebeden dispersiyonun etkisi zayıf iken soliton çözümlerinde simetri kırılması meydana gelmiştir ve ilgili γ değerine ait soliton çözümlerinin çatallanma grafiği gösterilmiştir. Dördüncü mertebeden dispersiyonun etkisi arttırıldıkça simetri kırılmasının baskılandığı gözlemlenmiştir. Daha sonra, ilgili CQNLS denkleminin sayısal olarak elde edilen soliton çözümlerinin doğrusal ve doğrusal olmayan kararlılık analizleri verilmiştir. Doğrusal kararlılıkları için soliton çözümlerinin doğrusal spektrumundaki özdeğerler incelenirken, doğrusal olmayan kararlılık analizi için soliton çözümleri ilerletilerek doğrusal olmayan evrimleri incelenmiştir.

Beşinci bölümde, çalışmada elde edilen tüm sonuçlar özetlenmiştir. Dördüncü mertebeden dispersiyonun, soliton çözümlerindeki simetri kırılmasını tamamen baskıladığı için pozitif etkisi olduğu sonucuna varılmıştır. Aynı şekilde, dördüncü mertebeden dispersiyonun etkisini arttırmanın doğrusal ve doğrusal olmayan olarak kararsız solitonları kararlı hale getirdiği gözlemlenmiştir. Dolayısıyla, kararlılık analizi için de oldukça güçlü ve pozitif yönde etkileri olduğundan bahsedilmiştir.

1. INTRODUCTION

Many natural phenomena are mathematically modeled using nonlinear partial differential equations. An extensive class of weakly nonlinear dispersive partial differential equations admits the traveling wave solutions that play a significant role in nonlinear wave propagation problems which are observed in various fields such as nonlinear optics, Bose-Einstein condensates, fluid dynamics, plasma physics, elastic media, and biology. A solitary wave or soliton is a special localized traveling wave solution, which is in the form of a wave packet or a pulse that can be propagated without any distortion at constant velocity. In the absence of nonlinearity, the dispersion can lead to destroying a solitary wave as various spectral components of the wave would propagate with different velocities, while the nonlinearity sharpens the solitary wave in the absence of dispersion, which leads to the breaking of pulses. Since solitons are formed due to the balance between the dispersive and nonlinear effects of the medium, they can maintain their shape during propagation [1–3].

In the context of nonlinear optics, soliton refers to any optical field that remains unchanged during propagation due to the balance between the medium's diffraction and the self-phase modulation [4, 5]. This property of optical solitons makes them ideal candidates for potential applications in optical fiber communications since they can propagate over long distances in fiber transmission systems. In 1973, Akira Hasegawa and Fred Tappert were the first to suggest that solitons can propagate inside an optical fiber that is a dispersive nonlinear medium [6, 7]. In 1980, the propagation of solitons in optical fibers was experimentally observed by Mollenauer et al. [8]. In recent years, optical solitons have been one of the most exciting research areas in modern communications. The current research of optical solitons and their considerable potential for technological applications are very important to the future of communications, and therefore of special interest.

The propagation of optical pulses inside optical fibers is governed by the nonlinear Schrödinger (NLS) equation as long as the pulse width exceeds roughly 1 picosecond [5]:

$$i\Psi_z + \Psi_{xx} + \alpha |\Psi|^2 \Psi = 0, \tag{1.1}$$

where $\Psi(x,z)$ is normalized complex-valued slowly varying pulse envelope of the electric field, z is the scaled propagation distance, x is the transverse coordinate, Ψ_{xx} corresponds to diffraction and α is the coefficient of the cubic (Kerr-type) nonlinearity of the medium. However, it is realized that not only second order (group-velocity) dispersion (GVD) but also third order dispersion (TOD) and fourth order dispersion (FOD) must be taken into account when ultrashort pulses are studied [9]. In other words, the cubic NLS equation does not govern the dynamics of ultra-short optical pulse (with durations of less than picosecond, which is equal to 10^{-12} of a second) propagation. For example, the approximation of the cubic NLS equation breaks down since solid state solitary laser pulses are generated with durations shorter than 10 femtoseconds (10^{-14} of a second). Therefore, to describe the dynamics in such systems, the higher-order diffraction or dispersion effects cannot be neglected. The TOD and higher-order dispersion need to be considered for performance enhancement over trans-oceanic and trans-continental distances. Moreover, for short pulse widths where the GVD changes, within the spectral bandwidth of the signal, FOD needs to be taken into account [10]. The generalized cubic NLS equation with an fourth order dispersion is given as

$$i\Psi_z + \Psi_{xx} - \gamma \Psi_{xxxx} + \alpha |\Psi|^2 \Psi = 0, \tag{1.2}$$

where, $\gamma > 0$ is the coupling constant of the fourth order dispersion. For $\alpha = 1$, Eq. (1.2) has an exact stationary solution [11]

$$\Psi(x,z) = \sqrt{\frac{3}{10\gamma}} \operatorname{sech}^2\left(\frac{x}{\sqrt{20\gamma}}\right) \exp\left(i\frac{4}{25\gamma}z\right). \tag{1.3}$$

The cubic NLS equation fails to the governing of the propagation of an electromagnetic wave in photorefractive materials [5]. Fibers made by using optical materials such as silicate and chalcogenide glasses are required higher-order nonlinearity. Therefore, the cubic-quintic nonlinear Schrödinger (CQNLS) equation comes into account [12]. However, it is well known that the soliton solutions to the (1+1)D NLS equation

that has nonlinearity stronger than cubic nonlinearity blow up during propagation at a finite distance z [5, 13]. This blow-up phenomenon, called wave collapse, refers to that the wave solutions can develop spikes of infinite amplitude in finite time or finite propagation distance [14]. Furthermore, adding an external potential to the governing model can arrest the wave collapse phenomenon and may be beneficial for performance enhancement [15–17].

Interest in parity-time ($\mathcal{PT}$) symmetric systems which originated from non-Hermitian quantum mechanics [18] has grown considerably over the past decade. If the optical waveguide includes energy gain and loss, the optical potential of the medium would be complex [19]. If this complex potential $V(x)$ is $\mathcal{PT}$-symmetric, it satisfies the condition $V^*(x) = V(-x)$ [20]. Physically, the real part of the $\mathcal{PT}$-symmetric potential corresponds to the refractive index of the medium while the imaginary part of the $\mathcal{PT}$-symmetric potential corresponds to the gain-loss profile. Moreover, its real and imaginary parts are even and odd functions, respectively [21].

One of the major unifying concepts in physics is symmetry. Symmetries determine the shapes, interactions, and evolutions that take place in nature. However, the states of a system do not always have the same symmetries as the theory that describes them, which is perhaps the most significant aspect of symmetry in physics theories. This kind of spontaneous breakdown of symmetries governs also the dynamics of phase transitions, the appearance of new particles and excitations, the rigidity of states of matter [22].

Spontaneous symmetry breaking occurs when the symmetric system is triggered by fluctuations to evolve toward one of its nonsymmetric states [23]. In nonlinear optics, the spontaneous symmetry breaking is also called symmetry-breaking bifurcation and symmetry-breaking bifurcation of solitons is a common phenomenon. Two branches of asymmetric solitons bifurcate from the base branch of symmetric solitons by a pitchfork bifurcation when the base branch's power crosses a specific threshold [19].

Just as most nonlinear wave phenomena in science and engineering are governed by nonintegrable equations [14], the equations governing the existence and dynamics of rich, complex, and interesting phenomena mentioned above can not be solved analytically because they are also nonintegrable. Therefore, numerical methods are

necessary to examine dynamics of these structures. In Chapter 2, we describe in detail numerical methods used for the computation of solitary wave solutions, and the calculation of the linear-stability spectrum of solitary waves.

1.1 Purpose of Thesis

In this thesis, the existence of symmetry breaking of optical solitons and suppression of symmetry-breaking bifurcations will be investigated in the optical system that is the nonlinear paraxial beam propagation in cubic-quintic nonlinearity with a complex $\mathcal{PT}$-symmetric potential and fourth order dispersion. This propagation is governed by the (1+1)D normalized CQNLS equation

$$i\Psi_z + \Psi_{xx} - \gamma\Psi_{xxxx} + V(x)\Psi + \alpha|\Psi|^2\Psi + \beta|\Psi|^4\Psi = 0, \tag{1.4}$$

where $\Psi(x,z)$ is normalized complex-valued slowly varying pulse envelope of the electric field, z is the scaled propagation distance, x is the transverse coordinate, $\gamma > 0$ is the coupling constant of the fourth order dispersion, $V(x) = V_{re}(x) + iV_{im}(x)$ represents a $\mathcal{PT}$-symmetric potential, α and β are the coefficients of cubic and quintic nonlinearity, respectively. To obtain the soliton solutions of the Eq. (1.4), the squared-operator method (described in Section 2.1) will be employed using the ansatz in the form of $\Psi(x,z) = \psi(x)e^{i\mu z}$, where ψ is a complex-valued localized function and μ is a real-valued propagation constant (or eigenvalue). As the external potential, we consider a special class of $\mathcal{PT}$-symmetric potentials that are of the form [24]

$$V(x) = g^2(x) + c_0 g(x) + ig'(x), \tag{1.5}$$

where $g(x)$ is an arbitrary real and even function, c_0 is arbitrary real constant. Even though symmetry breaking of $\mathcal{PT}$-symmetric solitons cannot occur in generic $\mathcal{PT}$-symmetric potentials [25], $\mathcal{PT}$-symmetric solitons can undergo a symmetry breaking for this special potential [19]. We take a localized double-hump function $g(x)$ in the form of

$$g(x) = A\left(e^{-(x+x_0)^2} + e^{-(x-x_0)^2}\right), \tag{1.6}$$

where A and x_0 are related to the modulation strength and separation of $\mathcal{PT}$-symmetric potential in Eq. (1.5), respectively. To examine the effect of fourth order dispersion on the existence and suppression of the symmetry breaking in the aforementioned

problem, the coefficient of fourth order dispersion γ will be gradually incremented. Then, the linear and nonlinear stability dynamics of the $\mathcal{PT}$-symmetric and non-$\mathcal{PT}$-symmetric solitons will be investigated by the corresponding linear-stability spectrum and nonlinear evolution, respectively.

1.2 Literature Review

Wave phenomena are observed in various areas in nature, with water waves and optical waves being two well-known examples. The diffraction in optics or dispersion in water waves is the main feature of linear wave phenomena. This feature causes the waves to disperse and disappear after a short time. In 1834, a type of water wave which moves without change of shape were accidentally discovered by John Scott Russell on the Union Canal. Russell called this phenomenon the Wave of Translation [26]. Russell carried out many experiments to obtain the properties of this wave but this observation contradicted the linear water wave theory. In 1895, Diederik Korteweg and Gustav de Vries noticed that a solitary wave which moves without change of shape can form due to the balance between the dispersion that causes a water wave to decay and nonlinear effects that can cause it to steepen. Consequently, Korteweg and de Vries derived the model equation describing the unidirectional propagation of waves in water of shallow depth. This equation is known as the Korteweg–de Vries (KdV) equation [27]. In 1965, Zabusky and Kruskal numerically obtained spatially periodic solutions of the KdV equation and named them solitary wave pulses or solitons. Moreover, they discovered that these solitary waves collided elastically, i.e., without loss of energy from the colliding pair [28]. In 1967, Gardner et al. invented the inverse scattering transform method and analytically solved the KdV equation, even though it is nonlinear. This transformation method breaks a nonlinear equation into two linear equations that can be simplified. In addition, many other nonlinear equations called integrable equations such as the NLS equation, the sine-Gordon equation, and the Kadomtsev–Petviashvili (KP) equation have soliton solutions and were solved by this method [29].

The NLS equation governing weakly nonlinear and dispersive wave packets in (1+1)D physical systems was first derived by Benney and Newell in 1967 [30]. Then, in 1968, Zakharov also derived the NLS equation when studying the modulational stability of finite amplitude periodic waves on the surface of a deep fluid [31]. In 1972, Zakharov

and Shabat solved exactly the NLS equation with the inverse scattering transform [32]. In 1973, Hasegawa and Tappert discovered that light pulse propagation in optical fibers is governed by the NLS equation and first suggested that optical solitons could be used in fiber optic communications [6, 7]. In 1980, Mollenauer et al. experimentally observed the propagation of solitons in optical fibers [8]. After that, optical solitons have become one of the most exciting research areas in modern communication, with the understanding of their properties and advantages in long-distance systems.

The evolution of the ultrashort optical pulses for cubic NLS equation in a nonlinear fiber including the fourth order dispersion was analyzed numerically and analytically by Karlsson and Höök [11]. Buryak and Akhmediev reported the existence of solitons with oscillating tails in their study that investigated the stability of bright solitons in an optical fiber with FOD. They demonstrated that oscillatory tails create a potential barrier in the interaction of two neighboring solitons, preventing them from approaching each other closer than a specific minimal distance. [33]. The dynamics and interactions of these solitons with oscillating tails were also investigated in [34].

Wave collapse in the NLS equation first observed numerically by Kelley in 1965 [35] and proved analytically by Vlasov et al. who developed the method of moments to determine the collapse distance [36]. In 1983, Weinstein proved that wave collapse cannot occur if the initial power of the wave is below the critical power [37]. Merle examined the collapse behavior of the NLS equation as well as that of other related equations [38]. In addition, Moll et al. experimentally investigated the observations of optical wave collapse in Kerr nonlinearity and showed that the amplitude of the wave increases as the spatial extent decreases in a self-similar profile [39]. It is also shown that the wave collapse phenomenon can be arrested by adding an external potential to the governing model, which may be beneficial for performance enhancement [15–17].

In order to obtain solitary wave solutions, various numerical methods have been developed. In 1976, Petviashvili introduced a spectral numerical method in order to construct localized solutions of the Kadomtsev–Petviashvili equation which is a generalization to two spatial dimensions of the one-dimensional KdV equation [40]. This method is based on taking the Fourier transform of the governing equation, determining a convergence factor, and then constructing the fixed point iteration scheme. It has been extended to find localized solutions in a wide variety of interesting

systems [41–45]. In 2005, Petviashvili's method was extended by Ablowitz and Musslimani [46] since the convergence factor of Petviashvili's method depends on the homogeneity of the nonlinear terms. They proposed the Spectral Renormalization (SR) method which compute soliton solutions in nonlinear waveguides which has higher-order nonlinearities with different homogeneities. However, these methods only converge to the ground states of a nonlinear wave systems and diverge for excited states. In 2007, Yang and Lakoba developed an iterative numerical method called the squared-operator method (SOM), which is guaranteed to converge for both the ground and excited states [47].

Musslimani et al. showed that $\mathcal{PT}$-symmetric potentials can support soliton solutions and also examined the stability and propagation dynamics of $\mathcal{PT}$-symmetric solitons in a self-focusing Kerr nonlinearity with $\mathcal{PT}$-symmetric potential [21]. Gagnon obtained a large set of exact traveling-wave solutions of the (1+1)D CQNLS equation [48]. Göksel et al. investigated the existence and stability properties of optical solitons of (1+1)D CQNLS equation with a $\mathcal{PT}$-symmetric potential. They obtained the soliton solutions to this equation both numerically (by using the SR method) and analytically. The linear and nonlinear stability properties of obtained solitons were examined through linear spectrum analysis and direct simulations, respectively [17].

In recent years, a considerable amount of research about the symmetry-breaking bifurcation of solitons has been studied. In 2014, Yang reported the symmetry breaking of solitons in the (1+1)D cubic NLS equation with a special classes of $\mathcal{PT}$-symmetric potentials (see Eq. (1.5)) [19]. Then, in 2019, Yang showed a new type of symmetry-breaking bifurcation in the CQNLS equation with the same $\mathcal{PT}$-symmetric potential. Even though the two bifurcated branches had the same stability in previous studies, the bifurcated branches of asymmetric solitons in this optical system exhibited opposite stability [49]. Moreover, the symmetry breaking have examined in (2+1)D cubic NLS with complex potential [50], and in saturable nonlinear media with $\mathcal{PT}$-symmetric potential [51]. Recently, in Ref. [52], it has been shown that the symmetry-breaking bifurcation can be suppressed by adjusting the coefficient of the saturable nonlinearity.

1.3 Hypothesis

In this thesis, we will numerically demonstrate the existence of optical solitons in a cubic-quintic medium with a special $\mathcal{PT}$-symmetric potential in the presence of fourth-order dispersion. It is hypothesized that the symmetry-breaking bifurcation of solitons can be suppressed by increasing the strength of the fourth-order dispersion, even if $\mathcal{PT}$-symmetric solitons undergo a symmetry breaking in the weak fourth-order dispersion. Moreover, we expect that the fourth order dispersion positively influences the linear and nonlinear stability properties of solitons.

2. NUMERICAL METHODS

Numerical computations play an important role in nonlinear wave phenomena that are mostly governed by nonintegrable equations. The governing equations of wave phenomena cannot be solved analytically, since they are nonintegrable. Therefore, numerical methods are necessary to compute the solitary wave solutions to these equations. Moreover, the stability dynamics of obtained solutions can be examined by numerical methods. In this chapter, we describe numerical methods to compute the soliton solutions and the linear-stability spectrum of solitons.

2.1 Squared-Operator Method

Various numerical methods have been used in order to obtain localized or solitary wave solutions, which are called solitons in the physical literature, such as the shooting method [53, 54], the self-consistency method which is also called the nonlinear Rayleigh–Ritz iteration method [55, 56], and Newton's iteration method [57, 58]. Although these methods are efficient and highly accurate or converge fast for one-dimensional problems, they do not apply to higher-dimensional problems [14, 59]. Furthermore, the Petviashvili method [40], the Spectral Renormalization method [16,17,46], and the Pseudospectral Renormalization method [60,61] which are modifications of the Petviashvili method, and the accelerated imaginary-time evolution method [62] are also used. However, these methods only converge to the ground states of nonlinear wave systems and diverge for excited states. Yang and Lakoba developed an iterative numerical method that is guaranteed to converge for both the ground states and the excited states. This method is called the squared-operator method (SOM). The idea of SOM is to iterate a modified differential equation whose linearization operator is square of the original equation together with a preconditioning (or acceleration) operator for the purpose of accelerating its convergence [47].

In this section, the SOM method is modified so that it can be applied to the (1+1)D cubic-quintic nonlinear Schrödinger (NLS) equation including fourth order dispersion

with an external potential. This equation is given by

$$i\Psi_z + \Psi_{xx} - \gamma\,\Psi_{xxxx} + V(x)\Psi + \alpha\,|\Psi|^2\Psi + \beta\,|\Psi|^4\Psi = 0, \tag{2.1}$$

see Eq. (1.4) for more detailed explanation. We assume the soliton solutions of Eq. (2.1) in the form of

$$\Psi(x,z) = \psi(x)e^{i\mu z}, \tag{2.2}$$

where ψ is a complex-valued localized function, $\lim_{x\to\mp\infty}\psi(x) = 0$, and $\mu > 0$ is a real-valued propagation constant (or soliton eigenvalue). The following set of equations is obtained by using the ansatz Eq. (2.2):

$$\begin{aligned}
&\Psi_z = i\mu\,\psi e^{i\mu z}\\
&\Psi_{xx} = \frac{d^2\psi}{dx^2}e^{i\mu z}\\
&\Psi_{xxxx} = \frac{d^4\psi}{dx^4}e^{i\mu z}\\
&\Psi^* = \psi^* e^{-i\mu z}\\
&|\Psi|^2 = \Psi\Psi^* = \psi e^{i\mu z}\psi^* e^{-i\mu z} = \psi\psi^* = |\psi|^2\\
&|\Psi|^4 = |\psi|^2|\psi|^2 = |\psi|^4
\end{aligned} \tag{2.3}$$

where $(\cdot)^*$ denotes complex conjugate. Substituting the set of equations in Eq. (2.3) into Eq. (2.1), the following nonlinear eigenequation for ψ is obtained

$$-\mu\,\psi e^{i\mu z} + \frac{d^2\psi}{dx^2}e^{i\mu z} - \gamma\frac{d^4\psi}{dx^4}e^{i\mu z} + V(x)\,\psi e^{i\mu z} + \alpha|\psi|^2\psi e^{i\mu z} + \beta|\psi|^4\psi e^{i\mu z} = 0. \tag{2.4}$$

After cancelling the exponential term in Eq. (2.4), we obtain

$$-\mu\,\psi + \frac{d^2\psi}{dx^2} - \gamma\frac{d^4\psi}{dx^4} + V(x)\,\psi + \alpha|\psi|^2\psi + \beta|\psi|^4\psi = 0. \tag{2.5}$$

Inserting $\psi(x) = \psi_{re}(x) + i\psi_{im}(x)$ and $V(x) = V_{re}(x) + iV_{im}(x)$ into Eq. (2.5) yields

$$\begin{aligned}
&-\mu\,(\psi_{re} + i\psi_{im}) + \frac{d^2\psi_{re}}{dx^2} + i\frac{d^2\psi_{im}}{dx^2} - \gamma\frac{d^4\psi_{re}}{dx^4} - i\gamma\frac{d^4\psi_{im}}{dx^4} + (V_{re} + iV_{im})\,(\psi_{re} + i\psi_{im})\\
&+ \alpha\left(\psi_{re}^2 + \psi_{im}^2\right)(\psi_{re} + i\psi_{im}) + \beta\left(\psi_{re}^2 + \psi_{im}^2\right)^2(\psi_{re} + i\psi_{im}) = 0.
\end{aligned} \tag{2.6}$$

After calculations, we have

$$\begin{aligned}
&-\mu\,\psi_{re} - i\mu\,\psi_{im} + \frac{d^2\psi_{re}}{dx^2} + i\frac{d^2\psi_{im}}{dx^2} - \gamma\frac{d^4\psi_{re}}{dx^4} - i\gamma\frac{d^4\psi_{im}}{dx^4} + V_{re}\psi_{re} + iV_{re}\psi_{im}\\
&+ iV_{im}\psi_{re} + i^2V_{im}\psi_{im} + \alpha\left(\psi_{re}^2 + \psi_{im}^2\right)\psi_{re} + i\alpha\left(\psi_{re}^2 + \psi_{im}^2\right)\psi_{im}\\
&+ \beta\left(\psi_{re}^2 + \psi_{im}^2\right)^2\psi_{re} + i\beta\left(\psi_{re}^2 + \psi_{im}^2\right)^2\psi_{im} = 0,
\end{aligned} \tag{2.7}$$

and Eq. (2.7) can be written as

$$
\begin{aligned}
&-\mu\psi_{re}+\frac{d^2\psi_{re}}{dx^2}-\gamma\frac{d^4\psi_{re}}{dx^4}+V_{re}\psi_{re}-V_{im}\psi_{im}+\alpha\left(\psi_{re}^2+\psi_{im}^2\right)\psi_{re}\\
&+\beta\left(\psi_{re}^2+\psi_{im}^2\right)^2\psi_{re}+i\left[-\mu\psi_{im}+\frac{d^2\psi_{im}}{dx^2}-\gamma\frac{d^4\psi_{im}}{dx^4}+V_{re}\psi_{im}\right.\\
&\left.+V_{\mathrm{im}}\,\psi_{re}+\alpha\left(\psi_{re}^2+\psi_{im}^2\right)\psi_{im}+\beta\left(\psi_{re}^2+\psi_{im}^2\right)^2\psi_{im}\right]=0.
\end{aligned}
\tag{2.8}
$$

Separating Eq. (2.8) into its real and imaginary parts, we get equations for the real functions ψ_{re} and ψ_{im} as

$$
\begin{aligned}
&-\mu\psi_{re}+\frac{d^2\psi_{re}}{dx^2}-\gamma\frac{d^4\psi_{re}}{dx^4}+V_{re}\psi_{re}-V_{im}\psi_{im}+\alpha\left(\psi_{re}^2+\psi_{im}^2\right)\psi_{re}\\
&+\beta\left(\psi_{re}^2+\psi_{im}^2\right)^2\psi_{re}=0,
\end{aligned}
\tag{2.9}
$$

$$
\begin{aligned}
&-\mu\psi_{im}+\frac{d^2\psi_{im}}{dx^2}-\gamma\frac{d^4\psi_{im}}{dx^4}+V_{re}\psi_{im}+V_{im}\psi_{re}+\alpha\left(\psi_{re}^2+\psi_{im}^2\right)\psi_{im}\\
&+\beta\left(\psi_{re}^2+\psi_{im}^2\right)^2\psi_{im}=0.
\end{aligned}
\tag{2.10}
$$

Then, Eq. (2.9) and Eq. (2.10) can be written in matrix form of

$$
\begin{bmatrix}
-\mu+\dfrac{d^2}{dx^2}-\gamma\dfrac{d^4}{dx^4}+V_{re} & -V_{im}\\
+\alpha\left(\psi_{re}^2+\psi_{im}^2\right) & \\
+\beta\left(\psi_{re}^2+\psi_{im}^2\right)^2 & \\
V_{im} & -\mu+\dfrac{d^2}{dx^2}-\gamma\dfrac{d^4}{dx^4}+V_{re}\\
 & +\alpha\left(\psi_{re}^2+\psi_{im}^2\right)\\
 & +\beta\left(\psi_{re}^2+\psi_{im}^2\right)^2
\end{bmatrix}
\begin{bmatrix}\psi_{re}\\ \psi_{im}\end{bmatrix}=\begin{bmatrix}0\\0\end{bmatrix}
\tag{2.11}
$$

or in a shorter form as $\boldsymbol{L_0 U}=0$, where $\boldsymbol{U}=[\psi_{re},\psi_{im}]^T$ is a vector and the superscript "T" represents the transpose of a vector. Hence, we obtain the operator $\boldsymbol{L_0}$ in the matrix form as following

$$
\boldsymbol{L_0}=\begin{bmatrix}(L_0)_1 & (L_0)_2\\ -(L_0)_2 & (L_0)_1\end{bmatrix},
\tag{2.12}
$$

where

$$
(L_0)_1=-\mu+\frac{d^2}{dx^2}-\gamma\frac{d^4}{dx^4}+V_{re}+\alpha(\psi_{re}^2+\psi_{im}^2)+\beta(\psi_{re}^2+\psi_{im}^2)^2,
\tag{2.13}
$$

$$
(L_0)_2=-V_{im}.
\tag{2.14}
$$

Now the operator $\boldsymbol{L_1}$ which denotes the linearized operator of $\boldsymbol{L_0 U}$ around the solution $\boldsymbol{U}$ must be obtained, i.e., $\boldsymbol{L_0}(\boldsymbol{U}+\tilde{\boldsymbol{U}})=\boldsymbol{L_1}\tilde{\boldsymbol{U}}+O(\tilde{\boldsymbol{U}}^2)$, where $\tilde{\boldsymbol{U}}=[\tilde{\psi}_{re},\tilde{\psi}_{im}]^T$ and

$\tilde{\psi}_{re}, \tilde{\psi}_{im} \ll 1$. In accordance with this purpose, we first consider that Eq. (2.9) and Eq. (2.10) are written as the general type of nonlinearities

$$-\mu\psi_{re} + \frac{d^2\psi_{re}}{dx^2} - \gamma\frac{d^4\psi_{re}}{dx^4} + V_{re}\psi_{re} - V_{im}\psi_{im} + F(\psi_{re}^2 + \psi_{im}^2)\psi_{re} = 0, \tag{2.15}$$

$$-\mu\psi_{im} + \frac{d^2\psi_{im}}{dx^2} - \gamma\frac{d^4\psi_{im}}{dx^4} + V_{re}\psi_{im} + V_{im}\psi_{re} + F(\psi_{re}^2 + \psi_{im}^2)\psi_{im} = 0, \tag{2.16}$$

where $F(\psi_{re}^2 + \psi_{im}^2) = \alpha(\psi_{re}^2 + \psi_{im}^2) + \beta(\psi_{re}^2 + \psi_{im}^2)^2$ for cubic-quintic nonlinearity. Then substituting perturbations $\psi_{re} + \tilde{\psi}_{re}$ and $\psi_{im} + \tilde{\psi}_{im}$, and using linear Taylor expansion yield

$$\begin{aligned} F(\psi_{re}^2 + \psi_{im}^2) &= F\left((\psi_{re} + \tilde{\psi}_{re})^2 + (\psi_{im} + \tilde{\psi}_{im})^2\right) \\ &= F\left(\psi_{re}^2 + 2\psi_{re}\tilde{\psi}_{re} + \tilde{\psi}_{re}^2 + \psi_{im}^2 + 2\psi_{im}\tilde{\psi}_{im} + \tilde{\psi}_{im}^2\right) \\ &\approx F\left(\psi_{re}^2 + 2\psi_{re}\tilde{\psi}_{re} + \psi_{im}^2 + 2\psi_{im}\tilde{\psi}_{im}\right) \\ &\approx F(\psi_{re}^2 + \psi_{im}^2) + 2(\psi_{re}\tilde{\psi}_{re} + \psi_{im}\tilde{\psi}_{im})F'_{(\psi_{re}^2+\psi_{im}^2)}(\psi_{re}^2 + \psi_{im}^2) \end{aligned} \tag{2.17}$$

where $F'_{(\psi_{re}^2+\psi_{im}^2)} = dF/d(\psi_{re}^2 + \psi_{im}^2)$. Hence, $F(\psi_{re}^2 + \psi_{im}^2)\psi_{re}$ and $F(\psi_{re}^2 + \psi_{im}^2)\psi_{im}$ can be linearized by adding perturbation as follows, respectively

$$\begin{aligned} F(\psi_{re}^2 + \psi_{im}^2)\psi_{re} &= F\left((\psi_{re} + \tilde{\psi}_{re})^2 + (\psi_{im} + \tilde{\psi}_{im})^2\right)(\psi_{re} + \tilde{\psi}_{re}) \\ &\approx \left[F(\psi_{re}^2 + \psi_{im}^2) + 2(\psi_{re}\tilde{\psi}_{re} + \psi_{im}\tilde{\psi}_{im})F'_{(\psi_{re}^2+\psi_{im}^2)}(\psi_{re}^2 + \psi_{im}^2)\right] \\ &\quad \cdot(\psi_{re} + \tilde{\psi}_{re}) \\ &\approx (\psi_{re} + \tilde{\psi}_{re})F(\psi_{re}^2 + \psi_{im}^2) \\ &\quad + 2(\psi_{re}^2\tilde{\psi}_{re} + \psi_{re}\psi_{im}\tilde{\psi}_{im})F'_{(\psi_{re}^2+\psi_{im}^2)}(\psi_{re}^2 + \psi_{im}^2) \\ &\quad + 2(\psi_{re}\tilde{\psi}_{re}^2 + \psi_{im}\tilde{\psi}_{im}\tilde{\psi}_{re})F'_{(\psi_{re}^2+\psi_{im}^2)}(\psi_{re}^2 + \psi_{im}^2) \\ &\approx (\psi_{re} + \tilde{\psi}_{re})F(\psi_{re}^2 + \psi_{im}^2) \\ &\quad + 2(\psi_{re}^2\tilde{\psi}_{re} + \psi_{re}\psi_{im}\tilde{\psi}_{im})F'_{(\psi_{re}^2+\psi_{im}^2)}(\psi_{re}^2 + \psi_{im}^2) \end{aligned} \tag{2.18}$$

and

$$
\begin{aligned}
F(\psi_{re}^2+\psi_{im}^2)\psi_{im} &= F\left((\psi_{re}+\tilde{\psi}_{re})^2+(\psi_{im}+\tilde{\psi}_{im})^2\right)(\psi_{im}+\tilde{\psi}_{im}) \\
&\approx \left[F(\psi_{re}^2+\psi_{im}^2)+2(\psi_{re}\tilde{\psi}_{re}+\psi_{im}\tilde{\psi}_{im})F^{'}_{(\psi_{re}^2+\psi_{im}^2)}(\psi_{re}^2+\psi_{im}^2)\right] \\
&\quad \cdot(\psi_{im}+\tilde{\psi}_{im}) \\
&\approx (\psi_{im}+\tilde{\psi}_{im})F(\psi_{re}^2+\psi_{im}^2) \\
&\quad +2(\psi_{re}\tilde{\psi}_{re}\psi_{im}+\psi_{im}^2\tilde{\psi}_{im})F^{'}_{(\psi_{re}^2+\psi_{im}^2)}(\psi_{re}^2+\psi_{im}^2) \\
&\quad +2(\psi_{re}\tilde{\psi}_{re}\tilde{\psi}_{im}+\psi_{im}\tilde{\psi}_{im}^2)F^{'}_{(\psi_{re}^2+\psi_{im}^2)}(\psi_{re}^2+\psi_{im}^2) \\
&\approx (\psi_{im}+\tilde{\psi}_{im})F(\psi_{re}^2+\psi_{im}^2) \\
&\quad +2(\psi_{re}\tilde{\psi}_{re}\psi_{im}+\psi_{im}^2\tilde{\psi}_{im})F^{'}_{(\psi_{re}^2+\psi_{im}^2)}(\psi_{re}^2+\psi_{im}^2).
\end{aligned}
\tag{2.19}
$$

Now, we can substitute Eq. (2.18) into Eq.(2.15) and Eq. (2.19) into Eq.(2.16) with perturbations $\psi_{re}+\tilde{\psi}_{re}$ and $\psi_{im}+\tilde{\psi}_{im}$. Then, only terms of $O(\tilde{\psi}_{re})$ and $O(\tilde{\psi}_{im})$ are retained, we get

$$
\begin{aligned}
&-\mu(\psi_{re}+\tilde{\psi}_{re})+\frac{d^2(\psi_{re}+\tilde{\psi}_{re})}{dx^2}-\gamma\frac{d^4(\psi_{re}+\tilde{\psi}_{re})}{dx^4}+V_{re}(\psi_{re}+\tilde{\psi}_{re})-V_{im}(\psi_{im}+\tilde{\psi}_{im}) \\
&+(\psi_{re}+\tilde{\psi}_{re})F(\psi_{re}^2+\psi_{im}^2)+2(\psi_{re}^2\tilde{\psi}_{re}+\psi_{re}\psi_{im}\tilde{\psi}_{im})F^{'}_{(\psi_{re}^2+\psi_{im}^2)}(\psi_{re}^2+\psi_{im}^2)=0,
\end{aligned}
\tag{2.20}
$$

$$
\begin{aligned}
&-\mu(\psi_{im}+\tilde{\psi}_{im})+\frac{d^2(\psi_{im}+\tilde{\psi}_{im})}{dx^2}-\gamma\frac{d^4(\psi_{im}+\tilde{\psi}_{im})}{dx^4}+V_{re}(\psi_{im}+\tilde{\psi}_{im})+V_{im}(\psi_{re}+\tilde{\psi}_{re}) \\
&+(\psi_{im}+\tilde{\psi}_{im})F(\psi_{re}^2+\psi_{im}^2)+2(\psi_{re}\tilde{\psi}_{re}\psi_{im}+\psi_{im}^2\tilde{\psi}_{im})F^{'}_{(\psi_{re}^2+\psi_{im}^2)}(\psi_{re}^2+\psi_{im}^2)=0.
\end{aligned}
\tag{2.21}
$$

Substituting $F(\psi_{re}^2+\psi_{im}^2)=\alpha(\psi_{re}^2+\psi_{im}^2)+\beta(\psi_{re}^2+\psi_{im}^2)^2 \Rightarrow F^{'}_{(\psi_{re}^2+\psi_{im}^2)}(\psi_{re}^2+\psi_{im}^2)=\alpha+2\beta(\psi_{re}^2+\psi_{im}^2)$ into Eq. (2.20) and Eq. (2.21) gives

$$
\begin{aligned}
&-\mu(\psi_{re}+\tilde{\psi}_{re})+\frac{d^2(\psi_{re}+\tilde{\psi}_{re})}{dx^2}-\gamma\frac{d^4(\psi_{re}+\tilde{\psi}_{re})}{dx^4}+V_{re}(\psi_{re}+\tilde{\psi}_{re}) \\
&-V_{im}(\psi_{im}+\tilde{\psi}_{im})+(\psi_{re}+\tilde{\psi}_{re})\left[\alpha(\psi_{re}^2+\psi_{im}^2)+\beta(\psi_{re}^2+\psi_{im}^2)^2\right] \\
&+2(\psi_{re}^2\tilde{\psi}_{re}+\psi_{re}\psi_{im}\tilde{\psi}_{im})\left[\alpha+2\beta(\psi_{re}^2+\psi_{im}^2)\right]=0,
\end{aligned}
\tag{2.22}
$$

$$
\begin{aligned}
&-\mu(\psi_{im}+\tilde{\psi}_{im})+\frac{d^2(\psi_{im}+\tilde{\psi}_{im})}{dx^2}-\gamma\frac{d^4(\psi_{im}+\tilde{\psi}_{im})}{dx^4}+V_{re}(\psi_{im}+\tilde{\psi}_{im}) \\
&+V_{im}(\psi_{re}+\tilde{\psi}_{re})+(\psi_{im}+\tilde{\psi}_{im})\left[\alpha(\psi_{re}^2+\psi_{im}^2)+\beta(\psi_{re}^2+\psi_{im}^2)^2\right] \\
&+2(\psi_{re}\tilde{\psi}_{re}\psi_{im}+\psi_{im}^2\tilde{\psi}_{im})\left[\alpha+2\beta(\psi_{re}^2+\psi_{im}^2)\right]=0.
\end{aligned}
\tag{2.23}
$$

After calculations and grouping the terms, Eq. (2.22) and Eq. (2.23) can be written as follows, respectively

$$\begin{aligned}
&\Big[-\mu\psi_{re}+\frac{d^2\psi_{re}}{dx^2}-\gamma\frac{d^4\psi_{re}}{dx^4}+V_{re}\psi_{re}-V_{im}\psi_{im}+\alpha\left(\psi_{re}^2+\psi_{im}^2\right)\psi_{re}\\
&+\beta\left(\psi_{re}^2+\psi_{im}^2\right)^2\psi_{re}\Big]+\Big[-\mu\tilde{\psi}_{re}+\frac{d^2\tilde{\psi}_{re}}{dx^2}-\gamma\frac{d^4\tilde{\psi}_{re}}{dx^4}+V_{re}\tilde{\psi}_{re}-V_{im}\tilde{\psi}_{im}\\
&+\alpha\left(\psi_{re}^2+\psi_{im}^2\right)\tilde{\psi}_{re}+\beta\left(\psi_{re}^2+\psi_{im}^2\right)^2\tilde{\psi}_{re}+2\alpha\psi_{re}^2\tilde{\psi}_{re}\\
&+4\beta\left(\psi_{re}^2+\psi_{im}^2\right)\psi_{re}^2\tilde{\psi}_{re}+2\alpha\psi_{re}\psi_{im}\tilde{\psi}_{im}+4\beta\left(\psi_{re}^2+\psi_{im}^2\right)\psi_{re}\psi_{im}\tilde{\psi}_{im}\Big]=0,
\end{aligned}\tag{2.24}$$

and

$$\begin{aligned}
&\Big[-\mu\psi_{im}+\frac{d^2\psi_{im}}{dx^2}-\gamma\frac{d^4\psi_{im}}{dx^4}+V_{re}\psi_{im}+V_{im}\psi_{re}+\alpha\left(\psi_{re}^2+\psi_{im}^2\right)\psi_{im}\\
&+\beta\left(\psi_{re}^2+\psi_{im}^2\right)^2\psi_{im}\Big]+\Big[-\mu\tilde{\psi}_{im}+\frac{d^2\tilde{\psi}_{im}}{dx^2}-\gamma\frac{d^4\tilde{\psi}_{im}}{dx^4}+V_{re}\tilde{\psi}_{im}+V_{im}\tilde{\psi}_{re}\\
&+\alpha\left(\psi_{re}^2+\psi_{im}^2\right)\tilde{\psi}_{im}+\beta\left(\psi_{re}^2+\psi_{im}^2\right)^2\tilde{\psi}_{im}+2\alpha\psi_{re}\psi_{im}\tilde{\psi}_{re}\\
&+4\beta\left(\psi_{re}^2+\psi_{im}^2\right)\psi_{re}\psi_{im}\tilde{\psi}_{re}+2\alpha\psi_{im}^2\tilde{\psi}_{im}+4\beta\left(\psi_{re}^2+\psi_{im}^2\right)\psi_{im}^2\tilde{\psi}_{im}\Big]=0.
\end{aligned}\tag{2.25}$$

As can be seen from Eq. (2.9) and Eq. (2.10), the first brackets of Eq. (2.24) and Eq. (2.25) are identically zero as $\boldsymbol{U}=[\psi_{re},\psi_{im}]^T$ is a solution of $\boldsymbol{L_0U}=0$. For Eqs. (2.24) and (2.25) to hold true, the second brackets of these equations must be equal to zero. Therefore, one gets

$$\begin{aligned}
&-\mu\tilde{\psi}_{re}+\frac{d^2\tilde{\psi}_{re}}{dx^2}-\gamma\frac{d^4\tilde{\psi}_{re}}{dx^4}+V_{re}\tilde{\psi}_{re}-V_{im}\tilde{\psi}_{im}+\alpha\left(\psi_{re}^2+\psi_{im}^2\right)\tilde{\psi}_{re}\\
&+\beta\left(\psi_{re}^2+\psi_{im}^2\right)^2\tilde{\psi}_{re}+2\alpha\psi_{re}^2\tilde{\psi}_{re}+4\beta\left(\psi_{re}^2+\psi_{im}^2\right)\psi_{re}^2\tilde{\psi}_{re}\\
&+2\alpha\psi_{re}\psi_{im}\tilde{\psi}_{im}+4\beta\left(\psi_{re}^2+\psi_{im}^2\right)\psi_{re}\psi_{im}\tilde{\psi}_{im}=0,
\end{aligned}\tag{2.26}$$

$$\begin{aligned}
&-\mu\tilde{\psi}_{im}+\frac{d^2\tilde{\psi}_{im}}{dx^2}-\gamma\frac{d^4\tilde{\psi}_{im}}{dx^4}+V_{re}\tilde{\psi}_{im}+V_{im}\tilde{\psi}_{re}+\alpha\left(\psi_{re}^2+\psi_{im}^2\right)\tilde{\psi}_{im}\\
&+\beta\left(\psi_{re}^2+\psi_{im}^2\right)^2\tilde{\psi}_{im}+2\alpha\psi_{re}\psi_{im}\tilde{\psi}_{re}+4\beta\left(\psi_{re}^2+\psi_{im}^2\right)\psi_{re}\psi_{im}\tilde{\psi}_{re}\\
&+2\alpha\psi_{im}^2\tilde{\psi}_{im}+4\beta\left(\psi_{re}^2+\psi_{im}^2\right)\psi_{im}^2\tilde{\psi}_{im}=0.
\end{aligned}\tag{2.27}$$

After calculations, Eq. (2.26) and Eq. (2.27) can be written as

$$\begin{aligned}
&-\mu\tilde{\psi}_{re}+\frac{d^2\tilde{\psi}_{re}}{dx^2}-\gamma\frac{d^4\tilde{\psi}_{re}}{dx^4}+V_{re}\tilde{\psi}_{re}-V_{im}\tilde{\psi}_{im}+3\alpha\psi_{re}^2\tilde{\psi}_{re}+\alpha\psi_{im}^2\tilde{\psi}_{re}+5\beta\psi_{re}^4\tilde{\psi}_{re}\\
&+6\beta\psi_{re}^2\psi_{im}^2\tilde{\psi}_{re}+\beta\psi_{im}^4\tilde{\psi}_{re}+2\alpha\psi_{re}\psi_{im}\tilde{\psi}_{im}+4\beta\psi_{re}^3\psi_{im}\tilde{\psi}_{im}+4\beta\psi_{re}\psi_{im}^3\tilde{\psi}_{im}=0,
\end{aligned}\tag{2.28}$$

and

$$-\mu\tilde{\psi}_{im}+\frac{d^2\tilde{\psi}_{im}}{dx^2}-\gamma\frac{d^4\tilde{\psi}_{im}}{dx^4}+V_{re}\tilde{\psi}_{im}+V_{im}\tilde{\psi}_{re}+\alpha\psi_{re}^2\tilde{\psi}_{im}+3\alpha\psi_{im}^2\tilde{\psi}_{im}+\beta\psi_{re}^4\tilde{\psi}_{im}$$
$$+6\beta\psi_{re}^2\psi_{im}^2\tilde{\psi}_{re}+\beta\psi_{im}^4\tilde{\psi}_{re}+2\alpha\psi_{re}\psi_{im}\tilde{\psi}_{im}+4\beta\psi_{re}^3\psi_{im}\tilde{\psi}_{im}+4\beta\psi_{re}\psi_{im}^3\tilde{\psi}_{im}=0, \tag{2.29}$$

respectively. Moreover, it is noticed that Eq. (2.24) and Eq. (2.25) satisfy $\boldsymbol{L_0}(\boldsymbol{U}+\tilde{\boldsymbol{U}})=\boldsymbol{L_1}\tilde{\boldsymbol{U}}+O(\tilde{\boldsymbol{U}}^2)$. Therefore, for the purpose of obtaining linearized operator $\boldsymbol{L_1}$, we can write Eq. (2.28) and Eq. (2.29) in the matrix form

$$\begin{bmatrix} -\mu+\frac{d^2}{dx^2}-\gamma\frac{d^4}{dx^4}+V_{re} & \\ +3\alpha\psi_{re}^2+\alpha\psi_{im}^2+5\beta\psi_{re}^4 & -V_{im}+2\alpha\psi_{re}\psi_{im} \\ +6\beta\psi_{re}^2\psi_{im}^2+\beta\psi_{im}^4 & +4\beta\psi_{re}^3\psi_{im}+4\beta\psi_{re}\psi_{im}^3 \\ & \\ V_{im}+2\alpha\psi_{re}\psi_{im} & -\mu+\frac{d^2}{dx^2}-\gamma\frac{d^4}{dx^4}+V_{re} \\ +4\beta\psi_{re}^3\psi_{im}+4\beta\psi_{re}\psi_{im}^3 & +\alpha\psi_{re}^2+3\alpha\psi_{im}^2+\beta\psi_{re}^4 \\ & +6\beta\psi_{re}^2\psi_{im}^2+5\beta\psi_{im}^4 \end{bmatrix}\begin{bmatrix}\tilde{\psi}_{re}\\ \\ \tilde{\psi}_{im}\end{bmatrix}=\begin{bmatrix}0\\ \\ 0\end{bmatrix}. \tag{2.30}$$

Consequently, from Eq. (2.30), the linearized operator $\boldsymbol{L_1}$ is obtained in the form of

$$\boldsymbol{L_1}=\begin{bmatrix}(L_1)_{11} & (L_1)_{12}\\ (L_1)_{21} & (L_1)_{22}\end{bmatrix}, \tag{2.31}$$

where the matrix elements of the linearized operator $\boldsymbol{L_1}$ can be expressed as

$$\begin{aligned}(L_1)_{11}&=-\mu+\frac{d^2}{dx^2}-\gamma\frac{d^4}{dx^4}+V_{re}+3\alpha\psi_{re}^2+\alpha\psi_{im}^2+5\beta\psi_{re}^4+6\beta\psi_{re}^2\psi_{im}^2+\beta\psi_{im}^4,\\ (L_1)_{12}&=-V_{im}+2\alpha\psi_{re}\psi_{im}+4\beta\psi_{re}^3\psi_{im}+4\beta\psi_{re}\psi_{im}^3,\\ (L_1)_{21}&=V_{im}+2\alpha\psi_{re}\psi_{im}+4\beta\psi_{re}^3\psi_{im}+4\beta\psi_{re}\psi_{im}^3,\\ (L_1)_{22}&=-\mu+\frac{d^2}{dx^2}-\gamma\frac{d^4}{dx^4}+V_{re}+\alpha\psi_{re}^2+3\alpha\psi_{im}^2+\beta\psi_{re}^4+6\beta\psi_{re}^2\psi_{im}^2+5\beta\psi_{im}^4.\end{aligned} \tag{2.32}$$

Here, we make use of the properties of the Fourier transform when constructing the iteration scheme with the operator $\boldsymbol{L_0}$ and the linearized operator $\boldsymbol{L_1}$ that we have obtained. The Fourier transform of an absolutely integrable function $f(x)$ is defined as

$$\mathcal{F}\{f(x)\}=\hat{f}(k_x)=\int_{-\infty}^{\infty}f(x)\,e^{-ik_xx}dx, \tag{2.33}$$

where $\mathcal{F}$ represents the Fourier transform and k_x is the Fourier transform variable. On the other hand, the inverse Fourier transform of the function $\hat{f}(k_x)$ which is also

absolutely integrable is defined by the integral

$$\mathcal{F}^{-1}\left\{\hat{f}(k_x)\right\} = f(x) = \frac{1}{2\pi}\int_{-\infty}^{\infty} \hat{f}(k_x)\, e^{ik_x x} dk_x. \tag{2.34}$$

Moreover, according to the differentiation property of Fourier transform

$$\mathcal{F}\left\{\frac{d^n}{(dx)^n} f(x)\right\} = (ik_x)^n \mathcal{F}\{f(x)\} = (ik_x)^n \hat{f}, \qquad n \in \mathbb{N}, \tag{2.35}$$

where $f(x)$ is an absolutely continuous differentiable function [63]. By applying the Fourier transform and using its differentiation formula, some differential equations in x-space can be transformed into algebraic equations in k_x-space, which are easier to solve. After obtaining the solution of the algebraic equation in k_x-space, its equivalent in x-space is obtained by the inverse Fourier transform, which is the solution of the differential equation. Considering all these properties, we first take the Fourier transforms of the elements of $\boldsymbol{L_0}$ which is given as matrix form in Eq. (2.12)

$$\mathcal{F}\{\boldsymbol{L_0}\} = \begin{bmatrix} \mathcal{F}\{(L_0)_1\} & \mathcal{F}\{(L_0)_2\} \\ \mathcal{F}\{-(L_0)_2\} & \mathcal{F}\{(L_0)_1\} \end{bmatrix}, \tag{2.36}$$

where

$$\mathcal{F}\{(L_0)_1\} = -\mu + (ik_x)^2 - \gamma(ik_x)^4 + \mathcal{F}\left\{V_{re} + \alpha(\psi_{re}^2 + \psi_{im}^2) + \beta(\psi_{re}^2 + \psi_{im}^2)^2\right\}, \tag{2.37}$$

$$\mathcal{F}\{(L_0)_2\} = \mathcal{F}\{-V_{im}\}. \tag{2.38}$$

Then, we have

$$\mathcal{F}\{(L_0)_1\} = -\mu - k_x^2 - \gamma k_x^4 + \mathcal{F}\left\{V_{re} + \alpha(\psi_{re}^2 + \psi_{im}^2) + \beta(\psi_{re}^2 + \psi_{im}^2)^2\right\}, \tag{2.39}$$

$$\mathcal{F}\{(L_0)_2\} = \mathcal{F}\{-V_{im}\}. \tag{2.40}$$

Applying the inverse Fourier transform to Eq. (2.39) and Eq. (2.40), we get

$$\begin{aligned}(T_0)_1 = \mathcal{F}^{-1}\{\mathcal{F}\{(L_0)_1\}\} = &-\mu + \mathcal{F}^{-1}\left\{-k_x^2 - \gamma k_x^4\right\} + V_{re} + \alpha(\psi_{re}^2 + \psi_{im}^2) \\ &+ \beta(\psi_{re}^2 + \psi_{im}^2)^2,\end{aligned} \tag{2.41}$$

$$(T_0)_2 = \mathcal{F}^{-1}\{\mathcal{F}\{(L_0)_2\}\} = -V_{im}. \tag{2.42}$$

Hereby, we can write the operator $\boldsymbol{T_0}$ that we have obtained by taking advantage of the Fourier transform in matrix form

$$\boldsymbol{T_0} = \begin{bmatrix} (T_0)_1 & (T_0)_2 \\ -(T_0)_2 & (T_0)_1 \end{bmatrix}, \tag{2.43}$$

where $(T_0)_1$ and $(T_0)_2$ are given in Eq. (2.41) and Eq. (2.42), respectively. In other words, the differential operator $\boldsymbol{L_0}$ has turned into a multiplication operator $\boldsymbol{T_0}$. Similarly, to find the form (which is obtained by using the advantages of the Fourier transform) of the linearized operator $\boldsymbol{L_1}$, we take the Fourier transforms of elements of $\boldsymbol{L_1}$ that are given as matrix form in Eq. (2.31)

$$\mathcal{F}\{\boldsymbol{L_1}\} = \begin{bmatrix} \mathcal{F}\{(L_1)_{11}\} & \mathcal{F}\{(L_1)_{12}\} \\ \mathcal{F}\{(L_1)_{21}\} & \mathcal{F}\{(L_1)_{22}\} \end{bmatrix}, \tag{2.44}$$

where

$$\begin{aligned} \mathcal{F}\{(L_1)_{11}\} =& -\mu + -k_x^2 - \gamma k_x^4 + \mathcal{F}\{V_{re} + 3\alpha\psi_{re}^2 + \alpha\psi_{im}^2 + 5\beta\psi_{re}^4 \\ &+ 6\beta\psi_{re}^2\psi_{im}^2 + \beta\psi_{im}^4\}, \\ \mathcal{F}\{(L_1)_{12}\} =& \mathcal{F}\{-V_{im} + 2\alpha\psi_{re}\psi_{im} + 4\beta\psi_{re}^3\psi_{im} + 4\beta\psi_{re}\psi_{im}^3\}, \\ \mathcal{F}\{(L_1)_{21}\} =& \mathcal{F}\{V_{im} + 2\alpha\psi_{re}\psi_{im} + 4\beta\psi_{re}^3\psi_{im} + 4\beta\psi_{re}\psi_{im}^3\}, \\ \mathcal{F}\{(L_1)_{22}\} =& -\mu - k_x^2 - \gamma k_x^4 + \mathcal{F}\{V_{re} + \alpha\psi_{re}^2 + 3\alpha\psi_{im}^2 + \beta\psi_{re}^4 \\ &+ 6\beta\psi_{re}^2\psi_{im}^2 + 5\beta\psi_{im}^4\}. \end{aligned} \tag{2.45}$$

By taking the inverse Fourier transform of equations in Eq. (2.45), we obtain

$$\begin{aligned} (T_1)_{11} =& \mathcal{F}^{-1}\{\mathcal{F}\{(L_1)_{11}\}\} = -\mu + \mathcal{F}^{-1}\{-k_x^2 - \gamma k_x^4\} + V_{re} + 3\alpha\psi_{re}^2 + \alpha\psi_{im}^2 \\ &+ 5\beta\psi_{re}^4 + 6\beta\psi_{re}^2\psi_{im}^2 + \beta\psi_{im}^4, \\ (T_1)_{12} =& \mathcal{F}^{-1}\{\mathcal{F}\{(L_1)_{12}\}\} = -V_{im} + 2\alpha\psi_{re}\psi_{im} + 4\beta\psi_{re}^3\psi_{im} + 4\beta\psi_{re}\psi_{im}^3, \\ (T_1)_{21} =& \mathcal{F}^{-1}\{\mathcal{F}\{(L_1)_{21}\}\} = V_{im} + 2\alpha\psi_{re}\psi_{im} + 4\beta\psi_{re}^3\psi_{im} + 4\beta\psi_{re}\psi_{im}^3, \\ (T_1)_{22} =& \mathcal{F}^{-1}\{\mathcal{F}\{(L_1)_{22}\}\} = -\mu + +\mathcal{F}^{-1}\{-k_x^2 - \gamma k_x^4\} + V_{re} + \alpha\psi_{re}^2 + 3\alpha\psi_{im}^2 \\ &+ \beta\psi_{re}^4 + 6\beta\psi_{re}^2\psi_{im}^2 + 5\beta\psi_{im}^4. \end{aligned} \tag{2.46}$$

Hence, the linearized operator $\boldsymbol{T_1}$ that the linearized operator $\boldsymbol{L_1}$ is turned into a multiplication operator by using properties of the Fourier transform can be written as

$$\boldsymbol{T_1} = \begin{bmatrix} (T_1)_{11} & (T_1)_{12} \\ (T_1)_{21} & (T_1)_{22} \end{bmatrix}, \tag{2.47}$$

where $(T_1)_{11}$, $(T_1)_{12}$, $(T_1)_{21}$ and $(T_1)_{22}$ are given in Eq. (2.46). To obtain the solution $\boldsymbol{U} = [\psi_{re}, \psi_{im}]^T$, we numerically integrate the following distance dependent squared-operator evolution equation

$$\boldsymbol{U}_z = -\boldsymbol{M}^{-1}\boldsymbol{T}_1^{\dagger}\boldsymbol{M}^{-1}\boldsymbol{T_0}\boldsymbol{U}, \tag{2.48}$$

where $(\cdot)^{\dagger}$ denotes the Hermitian of the operator and $\boldsymbol{M}$ is a real valued positive definite Hermitian preconditioning operator that is introduced to accelerate the convergence in

solving systems of linear algebraic equations. Since it is easily invertible using the Fourier transform, we take the preconditioning operator $\boldsymbol{M}$ to be in the form of the following

$$\boldsymbol{M} = \left(c - \frac{d^2}{dx^2} + \gamma \frac{d^4}{dx^4} \right) \mathrm{diag}\,(1,1)\,, \tag{2.49}$$

where $c > 0$ is an acceleration parameter to which one adds to make $\boldsymbol{M}$ positive definite and for parametrizing the numerical scheme. Taking the Fourier transform of $\boldsymbol{M}$ yields

$$\begin{aligned} \mathcal{F}\{\boldsymbol{M}\} &= \left(c - (ik_x)^2 + \gamma (ik_x)^4 \right) \mathrm{diag}\,(1,1) \\ &= \left(c + k_x^2 + \gamma k_x^4 \right) \mathrm{diag}\,(1,1)\,. \end{aligned} \tag{2.50}$$

Therefore, we have

$$\boldsymbol{M}^{-1}\boldsymbol{T_0}\boldsymbol{U} = \mathcal{F}^{-1}\left\{ (\mathcal{F}\{\boldsymbol{M}\})^{-1}\,\mathcal{F}\{\boldsymbol{T_0}\boldsymbol{U}\} \right\}, \tag{2.51}$$

and

$$\boldsymbol{M}^{-1}\boldsymbol{T}_1^{\dagger}\boldsymbol{M}^{-1}\boldsymbol{T_0}\boldsymbol{U} = \mathcal{F}^{-1}\left\{ (\mathcal{F}\{\boldsymbol{M}\})^{-1}\,\mathcal{F}\left\{ \boldsymbol{T}_1^{\dagger}\boldsymbol{M}^{-1}\boldsymbol{T_0}\boldsymbol{U} \right\} \right\}. \tag{2.52}$$

Using the forward Euler method, the solution $\boldsymbol{U} = [\psi_{re}, \psi_{im}]^T$ is computed by an iterative scheme as follows

$$\boldsymbol{U}_{n+1} = \boldsymbol{U}_n - \left[\boldsymbol{M}^{-1}\boldsymbol{T}_1^{\dagger}\boldsymbol{M}^{-1}\boldsymbol{T_0}\boldsymbol{U} \right]_{\boldsymbol{U}=\boldsymbol{U}_n} \Delta z, \tag{2.53}$$

where Δz is an auxiliary distance-step parameter. After obtaining the solution $\boldsymbol{U} = [\psi_{re}, \psi_{im}]^T$, the soliton solution $\psi(x) = \psi_{re}(x) + i\psi_{im}(x)$ of stationary Eq. (2.5) can be obtained by substituting ψ_{re} and ψ_{im} into $\psi(x)$. In Ref. [47], it has been demonstrated that the SOM algorithm converges to a solution for a wide range of nonlinear partial differential equations if the initial condition is sufficiently close to the exact solution and the distance-step Δz in the iteration scheme is less than a specific threshold value. To determine the $\mathcal{PT}$-symmetric and non-$\mathcal{PT}$-symmetric soliton solutions in this thesis, we use the initial condition taken as a Gaussian type function

$$\Psi(x,0) = R_0 e^{-(x-b_0)^2/2}, \tag{2.54}$$

where R_0 and b_0 are the initial amplitude and the center of position of the function, respectively. The computational domain is $-30 \le x \le 30$, discretized by 1024 grid points. The error is defined as the difference between successive iteration functions. Our convergence criterion is that the error is less than 10^{-10}:

$$E = \sqrt{\|U_{n+1} - U_n\|^2} < 10^{-10}. \tag{2.55}$$

Under this convergence criterion, we have obtained soliton solutions satisfying the stationary equation in Eq. (2.5) with an absolute error of less than 10^{-9}. Furthermore, as the strength of fourth order dispersion increases, non-$\mathcal{PT}$-symmetric solitons have not been obtained since they no longer satisfy the stationary equation. Hence, the symmetry-breaking bifurcation is suppressed (see Section 4.1).

2.2 Fourier Collocation Method

After we obtain a soliton solution, determining its linear stability spectrum is an essential problem (a detailed explanation will be given in Section 3.2). The linear stability spectrum consists of eigenvalues of the linear-stability operator of the solitary wave and can be obtained by using the Fourier collocation method. To describe the Fourier collocation method, we consider the (1+1)D NLS equation with general types of nonlinearities as an example

$$i\Psi_z + \Psi_{xx} + F\left(|\Psi|^2\right)\Psi = 0, \tag{2.56}$$

where $F(\cdot)$ is a real-valued function. Eq. (2.56) admits soliton solutions of the form $\Psi(x,z) = \psi(x)e^{i\mu z}$, where $\psi(x)$ is a localized complex-valued function, and μ is the propagation constant. We perturb the soliton solution $\psi(x)$ by normal modes to analyze its linear stability as follows

$$\Psi(x,z) = \left\{\psi(x) + \varepsilon[v(x) + w(x)]e^{\lambda z} + \varepsilon\left[v^*(x) - w^*(x)\right]e^{\lambda^* z}\right\}e^{i\mu z}, \tag{2.57}$$

where $\varepsilon \ll 1$, $v(x)$ and $w(x)$ are normal modes perturbations, and λ is the eigenvalue of this normal mode. Substituting Eq. (2.57) into Eq. (2.56) and neglecting terms of $O(\varepsilon^2)$, the following linear stability eigenvalue problem is obtained

$$L\Phi = \lambda\Phi, \tag{2.58}$$

where

$$L = i\begin{bmatrix} H_0 & \dfrac{d^2}{dx^2} + H_1 \\ \dfrac{d^2}{dx^2} + H_2 & -H_0 \end{bmatrix}, \quad \Phi = \begin{bmatrix} v \\ w \end{bmatrix}, \tag{2.59}$$

and

$$
\begin{aligned}
H_0 &= \frac{1}{2}\left(\psi^2 - \psi^{*2}\right) F_{|\psi|^2}\left(|\psi|^2\right), \\
H_1 &= -\mu + F\left(|\psi|^2\right) + \left[|\psi|^2 - \frac{1}{2}\left(\psi^2 + \psi^{*2}\right)\right] F_{|\psi|^2}\left(|\psi|^2\right), \\
H_2 &= -\mu + F\left(|\psi|^2\right) + \left[|\psi|^2 + \frac{1}{2}\left(\psi^2 + \psi^{*2}\right)\right] F_{|\psi|^2}\left(|\psi|^2\right).
\end{aligned} \tag{2.60}
$$

Now, we start applying the Fourier collocation method to obtain the whole spectrum of the linear-stability operator L that we have obtained in Eq. (2.58). The infinite x-axis is first truncated into a finite interval $[-L/2, L/2]$. Then, the eigenfunction $\Phi = [v, w]^T$, and the functions H_0, H_1 and H_2 are expanded into Fourier series

$$
v(x) = \sum_n a_n e^{inkx}, \quad w(x) = \sum_n b_n e^{inkx}, \tag{2.61}
$$

and

$$
H_j = \sum_n c_n^{(j)} e^{inkx}, \quad j = 0, 1, 2, \tag{2.62}
$$

where $k = 2\pi/L$. Inserting the expansions in Eq. (2.61) and Eq. (2.62) into the linear stability eigenvalue problem in Eq. (2.58), an eigenvalue system is obtained for the coefficients a_j and b_j:

$$
\begin{aligned}
\sum_n c_n^{(0)} a_{j-n} - (kj)^2 b_j + \sum_n c_n^{(1)} b_{j-n} &= -i\lambda a_j, \\
-(kj)^2 a_j + \sum_n c_n^{(2)} a_{j-n} - \sum_n c_n^{(0)} b_{j-n} &= -i\lambda b_j,
\end{aligned} \tag{2.63}
$$

where $-\infty < j < \infty$. We truncate the number of Fourier modes to $-N < j < N$ and the following finite dimensional eigenvalue problem is obtained:

$$
i \begin{bmatrix} \mathcal{C}_0 & \mathcal{D} + \mathcal{C}_1 \\ \mathcal{D} + \mathcal{C}_2 & -\mathcal{C}_0 \end{bmatrix} \begin{bmatrix} A \\ B \end{bmatrix} = \lambda \begin{bmatrix} A \\ B \end{bmatrix}, \tag{2.64}
$$

where

$$
\mathcal{D} = (ik)^2 \operatorname{diag}(-N, -N+1, \ldots, N-1, N)^2, \tag{2.65}
$$

and the matrices $\mathcal{C}_0$, $\mathcal{C}_1$ and $\mathcal{C}_2$ are in the following form:

$$
\mathcal{C} = \begin{bmatrix}
c_0 & c_{-1} & \cdots & c_{-N} & & & \\
c_1 & c_0 & c_{-1} & \ddots & \ddots & & \\
\vdots & c_1 & c_0 & \ddots & \ddots & \ddots & \\
c_N & \ddots & \ddots & \ddots & \ddots & \ddots & c_{-N} \\
 & c_N & \ddots & \ddots & \ddots & \ddots & \vdots \\
 & & \ddots & \ddots & \ddots & \ddots & c_{-1} \\
 & & & & & & \\
 & & & c_N & \cdots & c_1 & c_0
\end{bmatrix}. \tag{2.66}
$$

The coefficients c_n takes the values $c_n^{(j)}$ for the matrix $\mathcal{C}_j$, and

$$A = \begin{bmatrix} a_{-N} \\ a_{-N+1} \\ \vdots \\ a_N \end{bmatrix}, \quad B = \begin{bmatrix} b_{-N} \\ b_{-N+1} \\ \vdots \\ b_N \end{bmatrix}. \tag{2.67}$$

The eigenvalue problem (2.64) can be solved by the QR algorithm which gives all the eigenvalues of the matrix [64]. It is noted that we can also obtain the corresponding eigenfunctions. In this thesis, the **"eig"** function in MATLAB is used, which is the command of the QR algorithm.

3. STABILITY ANALYSIS

Examining the stability of soliton is significant for understanding the dynamics of the physical system since it can suffer from collapse during propagation at a finite distance. In this chapter, we will explain how the linear and nonlinear stability dynamics of the numerically obtained solitons are analyzed.

3.1 Nonlinear Stability

A soliton that preserves its shape, location, and maximum amplitude during nonlinear evolution is considered nonlinearly stable. To examine the nonlinear stability of obtained solitons, we consider the nonlinear evolution simulations of these solitons by employing the split-step Fourier method in long distance.

We consider Eq. (1.4) in the following form which is multiplied by i

$$-\Psi_z + i\left(\Psi_{xx} - \gamma\Psi_{xxxx}\right) + i\left(V(x) + \alpha|\Psi|^2 + \beta|\Psi|^4\right)\Psi = 0, \tag{3.1}$$

and it can be written as

$$\Psi_z = i\left(\Psi_{xx} - \gamma\Psi_{xxxx}\right) + i\left(V(x) + \alpha|\Psi|^2 + \beta|\Psi|^4\right)\Psi. \tag{3.2}$$

Eq. (3.2) can be considered as $\Psi_z = M(\Psi) + N(\Psi)$. Then, we have two split equations to be solved:

$$\frac{\partial\Psi_M}{\partial z} = i\left(\partial_{xx} - \gamma\partial_{xxxx}\right)\Psi_M, \tag{3.3}$$

and

$$\frac{\partial\Psi_N}{\partial z} = i\left(V(x) + \alpha|\Psi|^2 + \beta|\Psi|^4\right)\Psi_N, \tag{3.4}$$

where are the linear and nonlinear parts, respectively. We take the Fourier transform of both sides of Eq. (3.3) as this split equation has an analytical solution in the frequency domain. Therefore, we obtain

$$\frac{\partial\hat{\Psi}_M}{\partial z} = i\left((ik_x)^2 - \gamma(ik_x)^4\right)\hat{\Psi}_M = -i\left(k_x^2 + \gamma k_x^4\right)\hat{\Psi}_M. \tag{3.5}$$

Eq. (3.5) is an ordinary differential equation of $\hat{\Psi}_M$ whose exact solution in the frequency domain is

$$\hat{\Psi}_M(k_x,z) = \hat{\Psi}_M(k_x,0)e^{-i\left(k_x^2+\gamma k_x^4\right)z}. \tag{3.6}$$

Taking the inverse Fourier transform of Eq. (3.6), we can obtain the exact solution of Eq. (3.3)

$$\Psi_M(x,z) = \mathcal{F}^{-1}\left(\hat{\Psi}_M(k_x,0)e^{-i\left(k_x^2+\gamma k_x^4\right)z}\right). \tag{3.7}$$

The nonlinear split equation in Eq. (3.4) has the exact solution

$$\Psi_N(x,z) = \Psi_N(x,0)e^{i\left(V(x)+\alpha|\Psi|^2+\beta|\Psi|^4\right)z}. \tag{3.8}$$

In this thesis, the fourth-order split-step Fourier method is employed with these obtained exact solutions of the split equations to examine the nonlinear stability of solitons. We take the initial condition to be numerically obtained solitons by the SOM over the computational domain $-30 \leq x \leq 30$, discretized by 1024 grid points. In addition, the distance step is taken as $\Delta z = 0.00025$.

3.2 Linear Stability

The linear stability will be analyzed by examining the linear spectrum of the soliton's linear stability operator.

3.2.1 Linear spectrum

We examine the linear stability spectrum of the soliton solution to consider the behavior of a soliton solution under small perturbations. Linear stability spectrum, which is also called linear spectrum, is the set of eigenvalues of the linear stability operator of a soliton and these eigenvalues give important information on the linear stability and other aspects of the soliton solution. If any of the calculated eigenvalues in the spectrum has a positive real part, then the soliton solution $\psi(x,z)$ is linearly unstable and it will grow exponentially with z. Moreover, the maximal growth rate of the perturbation instability is measured by the largest real part of the eigenvalues. Otherwise, the soliton solution is linearly stable. For instance, if the spectrum contains only purely imaginary discrete eigenvalues, the perturbations will only cause oscillations to the soliton solution [14]. In this subsection, we obtain the linear stability

operator of the soliton solutions, and then, the continuous spectrum of the linear stability eigenvalue problem is obtained.

To derive the linearization of (1+1)D cubic-quintic NLS equation including fourth order dispersion with an external potential given in Eq. (2.1), consider its general type of nonlinearities as follows:

$$i\Psi_z + \Psi_{xx} - \gamma\Psi_{xxxx} + V(x)\Psi + F(|\Psi|^2)\Psi = 0, \tag{3.9}$$

where $F(\cdot) \in \mathbb{R}$ and $F(0) = 0$. As we suggested before in Section 2.1, using the soliton solution of the form $\Psi(x,z) = \psi(x)e^{i\mu z}$ which Eq. (3.9) admits, we have the following expressions:

$$\begin{aligned}
&\Psi_z = i\mu\psi e^{i\mu z} \\
&\Psi_{xx} = \frac{d^2\psi}{dx^2}e^{i\mu z} \\
&\Psi_{xxxx} = \frac{d^4\psi}{dx^4}e^{i\mu z} \\
&\Psi^* = \psi^* e^{-i\mu z} \\
&|\Psi|^2 = \Psi\Psi^* = \psi e^{i\mu z}\psi^* e^{-i\mu z} = \psi\psi^* = |\psi|^2,
\end{aligned} \tag{3.10}$$

where $\psi(x)$ is a complex-valued function, $\lim_{x\to\mp\infty}\psi(x) = 0$. Substituting expressions in Eq. (3.10) into Eq. (3.9), we obtain the following eigenequation with a general type of nonlinearities

$$-\mu\psi e^{i\mu z} + \frac{d^2\psi}{dx^2}e^{i\mu z} - \gamma\frac{d^4\psi}{dx^4}e^{i\mu z} + V(x)\psi e^{i\mu z} + F(|\psi|^2)\psi e^{i\mu z} = 0. \tag{3.11}$$

In order to eliminate the exponential term, we multiply Eq. (3.11) by $e^{-i\mu z}$ and obtain

$$-\mu\psi + \frac{d^2\psi}{dx^2} - \gamma\frac{d^4\psi}{dx^4} + V(x)\psi + F(|\psi|^2)\psi = 0. \tag{3.12}$$

To determine the linear stability spectrum of obtained soliton solution, it is perturbed as follows

$$\Psi(x,z) = \left[\psi(x) + \varepsilon\left(g(x)e^{\lambda z} + h^*(x)e^{\lambda^* z}\right)\right]e^{i\mu z}, \tag{3.13}$$

where $\varepsilon \ll 1$, $g(x)$ and $h(x)$ are perturbation eigenfunctions and λ is the eigenvalue. For the purpose of inserting this perturbed solution into Eq. (3.9), the following

expressions are obtained

$$\begin{aligned}\Psi_z =& \frac{\partial}{\partial z}\left(\psi(x)+\varepsilon\left(g(x)e^{\lambda z}+h^*(x)e^{\lambda^* z}\right)\right)e^{i\mu z}\\ &+\left[\psi(x)+\varepsilon\left(g(x)e^{\lambda z}+h^*(x)e^{\lambda^* z}\right)\right]\frac{d}{dz}\left(e^{i\mu z}\right)\\ =&\varepsilon\left(\lambda g e^{\lambda z}+\lambda^* h^* e^{\lambda^* z}\right)e^{i\mu z}+\left[\psi+\varepsilon\left(g e^{\lambda z}+h^* e^{\lambda^* z}\right)\right]i\mu e^{i\mu z}\\ =&\left[\varepsilon\lambda g e^{\lambda z}+\varepsilon\lambda^* h^* e^{\lambda^* z}+i\mu\psi+i\mu\varepsilon g e^{\lambda z}+i\mu\varepsilon h^* e^{\lambda^* z}\right]e^{i\mu z},\end{aligned} \tag{3.14}$$

$$\begin{aligned}\Psi_{xx} &= \left[\frac{d^2\psi}{dx^2}+\varepsilon\frac{d^2 g}{dx^2}e^{\lambda z}+\varepsilon\frac{d^2 h^*}{dx^2}e^{\lambda^* z}\right]e^{i\mu z},\\ \Psi_{xxxx} &= \left[\frac{d^4\psi}{dx^4}+\varepsilon\frac{d^4 g}{dx^4}e^{\lambda z}+\varepsilon\frac{d^4 h^*}{dx^4}e^{\lambda^* z}\right]e^{i\mu z}.\end{aligned} \tag{3.15}$$

Neglecting terms of $O(\varepsilon^2)$ yields

$$\begin{aligned}|\Psi|^2=\Psi\Psi^* &= \left[\psi+\varepsilon\left(g e^{\lambda z}+h^* e^{\lambda^* z}\right)\right]e^{i\mu z}\left[\psi^*+\varepsilon\left(g^* e^{\lambda^* z}+h e^{\lambda z}\right)\right]e^{-i\mu z}\\ &=\psi\psi^*+\varepsilon\psi g^* e^{\lambda^* z}+\varepsilon\psi h e^{\lambda z}+\varepsilon\psi^* g e^{\lambda z}+\varepsilon^2 g g^* e^{(\lambda+\lambda^*)z}\\ &\quad+\varepsilon^2 g h e^{2\lambda z}+\varepsilon\psi^* h^* e^{\lambda^* z}+\varepsilon^2 g^* h^* e^{2\lambda^* z}+\varepsilon^2 h h^* e^{(\lambda+\lambda^*)z}\\ &\simeq|\psi|^2+\varepsilon\left(g^* e^{\lambda^* z}+h e^{\lambda z}\right)\psi+\varepsilon\left(g e^{\lambda z}+h^* e^{\lambda^* z}\right)\psi^*.\end{aligned} \tag{3.16}$$

Expanding $F(|\Psi|^2)$ into linear Taylor series expansion, which is $F(x+a)=F(x)+aF'(x)+O(a^2)$, we get

$$\begin{aligned}F\left(|\Psi|^2\right) &= F\left(|\psi|^2+\varepsilon\left(g^* e^{\lambda^* z}+h e^{\lambda z}\right)\psi+\varepsilon\left(g e^{\lambda z}+h^* e^{\lambda^* z}\right)\psi^*\right)\\ &\simeq F(|\psi|^2)+\left[\varepsilon\left(g^* e^{\lambda^* z}+h e^{\lambda z}\right)\psi+\varepsilon\left(g e^{\lambda z}+h^* e^{\lambda^* z}\right)\psi^*\right]F'\left(|\psi|^2\right).\end{aligned} \tag{3.17}$$

Therefore,

$$\begin{aligned}F\left(|\Psi|^2\right)\Psi =& \left\{F(|\psi|^2)+\left[\varepsilon\left(g^* e^{\lambda^* z}+h e^{\lambda z}\right)\psi+\varepsilon\left(g e^{\lambda z}+h^* e^{\lambda^* z}\right)\psi^*\right]F'\left(|\psi|^2\right)\right\}\\ &\cdot\left[\psi+\varepsilon\left(g e^{\lambda z}+h^* e^{\lambda^* z}\right)\right]e^{i\mu z}\\ =&\left\{\begin{array}{l}F(|\psi|^2)\psi+\varepsilon F(|\psi|^2)g e^{\lambda z}+\varepsilon F(|\psi|^2)h^* e^{\lambda^* z}\\ +\left(\begin{array}{l}\varepsilon\left(g^* e^{\lambda^* z}+h e^{\lambda z}\right)\psi^2\\ +\varepsilon\left(g e^{\lambda z}+h^* e^{\lambda^* z}\right)|\psi|^2\end{array}\right)F'(|\psi|^2)\\ +\left(\begin{array}{l}\varepsilon^2\left(|g|^2 e^{(\lambda+\lambda^*)z}+g h e^{2\lambda z}\right)\psi\\ +\varepsilon^2\left(g^2 e^{2\lambda z}+g h^* e^{(\lambda+\lambda^*)z}\right)\psi^*\end{array}\right)F'(|\psi|^2)\\ +\left(\begin{array}{l}\varepsilon^2\left(g^* h^* e^{2\lambda^* z}+|h|^2 e^{(\lambda+\lambda^*)z}\right)\psi\\ +\varepsilon^2\left(g h^* e^{(\lambda+\lambda^*)z}+(h^*)^2 e^{2\lambda^* z}\right)\psi^*\end{array}\right)F'(|\psi|^2)\end{array}\right\}e^{i\mu z}\end{aligned} \tag{3.18}$$

If only terms of $O(\varepsilon)$ are retained, one gets

$$F\left(|\Psi|^2\right)\Psi \simeq \left.\begin{array}{l} F\left(|\psi|^2\right)\left[\psi+\varepsilon\left(ge^{\lambda z}+h^*e^{\lambda^* z}\right)\right] \\ +F'\left(|\psi|^2\right)\left[\varepsilon\left(\psi^2 h+|\psi|^2 g\right)e^{\lambda z}+\varepsilon\left(\psi^2 g^*+|\psi|^2 h^*\right)e^{\lambda^* z}\right] \end{array}\right\} e^{i\mu z}. \tag{3.19}$$

Substituting Eq. (3.13), (3.14), (3.15) and (3.19) into Eq. (3.9) gives

$$\begin{aligned} & i\left(\varepsilon\lambda g e^{\lambda z}+\varepsilon\lambda^* h^* e^{\lambda^* z}+i\mu\psi+i\mu\varepsilon g e^{\lambda z}+i\mu\varepsilon h^* e^{\lambda^* z}\right)e^{i\mu z} \\ & +\left[\frac{d^2\psi}{dx^2}+\varepsilon\frac{d^2 g}{dx^2}e^{\lambda z}+\varepsilon\frac{d^2 h^*}{dx^2}e^{\lambda^* z}\right]e^{i\mu z}-\gamma\left[\frac{d^4\psi}{dx^4}+\varepsilon\frac{d^4 g}{dx^4}e^{\lambda z}+\varepsilon\frac{d^4 h^*}{dx^4}e^{\lambda^* z}\right]e^{i\mu z} \\ & +V\left[\psi+\varepsilon\left(ge^{\lambda z}+h^*e^{\lambda^* z}\right)\right]e^{i\mu z}+\left\{F\left(|\psi|^2\right)\left[\psi+\varepsilon\left(ge^{\lambda z}+h^*e^{\lambda^* z}\right)\right]\right. \\ & \left.+F'\left(|\psi|^2\right)\left[\varepsilon\left(\psi^2 h+|\psi|^2 g\right)e^{\lambda z}+\varepsilon\left(\psi^2 g^*+|\psi|^2 h^*\right)e^{\lambda^* z}\right]\right\}e^{i\mu z}=0. \end{aligned} \tag{3.20}$$

Eq. (3.20) is multiplied by $e^{-i\mu z}$, and the terms that have the same exponential factors are grouped. Hence, the following equation is obtained:

$$\begin{aligned} & \left[-\mu\psi+\frac{d^2\psi}{dx^2}-\gamma\frac{d^4\psi}{dx^4}+V\psi+F\left(|\psi|^2\right)\psi\right] \\ & +\varepsilon\left[i\lambda g-\mu g+\frac{d^2 g}{dx^2}-\gamma\frac{d^4 g}{dx^4}+Vg+F\left(|\psi|^2\right)g+\left(\psi^2 h+|\psi|^2 g\right)F'\left(|\psi|^2\right)\right]e^{\lambda z} \\ & +\varepsilon\left[\begin{array}{l} i\lambda^* h^*-\mu h^*+\dfrac{d^2 h^*}{dx^2}-\gamma\dfrac{d^4 h^*}{dx^4}+Vh^*+F\left(|\psi|^2\right)h^* \\ +\left(\psi^2 g^*+|\psi|^2 h^*\right)F'\left(|\psi|^2\right) \end{array}\right]e^{\lambda^* z}=0. \end{aligned} \tag{3.21}$$

As can be seen from Eq. (3.12), we know that the first bracket in Eq. (3.21) is identically equal to zero, since $\psi(x)$ is a solution for $z=0$. Consequently, the factors of $e^{\lambda z}$ and $e^{\lambda^* z}$ exponential terms must be equal to zero simultaneously, for Eq. (3.21) to be satisfied. Hereby, from the second bracket, we get

$$i\lambda g-\mu g+\frac{d^2 g}{dx^2}-\gamma\frac{d^4 g}{dx^4}+Vg+F\left(|\psi|^2\right)g+\left(\psi^2 h+|\psi|^2 g\right)F'\left(|\psi|^2\right)=0, \tag{3.22}$$

which can be rewritten as

$$\frac{d^2 g}{dx^2}-\gamma\frac{d^4 g}{dx^4}+\left[-\mu+V+F\left(|\psi|^2\right)+F'\left(|\psi|^2\right)|\psi|^2\right]g+F'\left(|\psi|^2\right)\psi^2 h=-i\lambda g, \tag{3.23}$$

and on the other hand, we have from the last bracket in Eq. (3.21),

$$i\lambda^* h^*-\mu h^*+\frac{d^2 h^*}{dx^2}-\gamma\frac{d^4 h^*}{dx^4}+Vh^*+F\left(|\psi|^2\right)h^*+\left(\psi^2 g^*+|\psi|^2 h^*\right)F'\left(|\psi|^2\right)=0, \tag{3.24}$$

which can be rewritten as

$$\frac{d^2h^*}{dx^2}-\gamma\frac{d^4h^*}{dx^4}+\left[-\mu+V+F\left(|\psi|^2\right)+F'\left(|\psi|^2\right)|\psi|^2\right]h^*+F'\left(|\psi|^2\right)\psi^2g^*=-i\lambda^*h^*. \tag{3.25}$$

Taking the complex conjugate of Eq. (3.25) yields

$$\frac{d^2h}{dx^2}-\gamma\frac{d^4h}{dx^4}+\left[-\mu+V^*+F\left(|\psi|^2\right)+F'\left(|\psi|^2\right)|\psi|^2\right]h+F'\left(|\psi|^2\right)(\psi^2)^*g=i\lambda h. \tag{3.26}$$

Then, Eq. (3.26) is multiplied by -1, and the following equation is obtained

$$-\frac{d^2h}{dx^2}+\gamma\frac{d^4h}{dx^4}+\left[\mu-V^*-F\left(|\psi|^2\right)-F'\left(|\psi|^2\right)|\psi|^2\right]h-F'\left(|\psi|^2\right)(\psi^2)^*g=-i\lambda h. \tag{3.27}$$

For convenience, we introduce the variable transformation:

$$g(x)=v(x)+w(x),\quad h(x)=v(x)-w(x). \tag{3.28}$$

Eq. (3.23) and Eq. (3.27) are written by using the above variable transformation

$$\begin{aligned}&\left(\frac{d^2v}{dx^2}+\frac{d^2w}{dx^2}\right)-\gamma\left(\frac{d^4v}{dx^4}+\frac{d^4w}{dx^4}\right)+\left[-\mu+V+F\left(|\psi|^2\right)+F'\left(|\psi|^2\right)|\psi|^2\right](v+w)\\&+F'\left(|\psi|^2\right)\psi^2(v-w)=-i\lambda(v+w),\end{aligned} \tag{3.29}$$

and

$$\begin{aligned}&-\left(\frac{d^2v}{dx^2}-\frac{d^2w}{dx^2}\right)+\gamma\left(\frac{d^4v}{dx^4}-\frac{d^4w}{dx^4}\right)+\left[\mu-V^*-F\left(|\psi|^2\right)-F'\left(|\psi|^2\right)|\psi|^2\right](v-w)\\&-F'\left(|\psi|^2\right)(\psi^2)^*(v+w)=-i\lambda(v-w),\end{aligned} \tag{3.30}$$

respectively. Then, we have

$$\begin{aligned}&\frac{d^2v}{dx^2}-\gamma\frac{d^4v}{dx^4}+\left[-\mu+V+F\left(|\psi|^2\right)+F'\left(|\psi|^2\right)|\psi|^2\right]v+F'\left(|\psi|^2\right)\psi^2v\\&+\frac{d^2w}{dx^2}-\gamma\frac{d^4w}{dx^4}+\left[-\mu+V+F\left(|\psi|^2\right)+F'\left(|\psi|^2\right)|\psi|^2\right]w-F'\left(|\psi|^2\right)\psi^2w\\&=-i\lambda v-i\lambda w,\end{aligned} \tag{3.31}$$

and

$$\begin{aligned}&-\frac{d^2v}{dx^2}+\gamma\frac{d^4v}{dx^4}+\left[\mu-V^*-F\left(|\psi|^2\right)-F'\left(|\psi|^2\right)|\psi|^2\right]v-F'\left(|\psi|^2\right)(\psi^2)^*v\\&+\frac{d^2w}{dx^2}-\gamma\frac{d^4w}{dx^4}+\left[-\mu+V^*+F\left(|\psi|^2\right)+F'\left(|\psi|^2\right)|\psi|^2\right]w-F'\left(|\psi|^2\right)(\psi^2)^*w\\&=-i\lambda v+i\lambda w.\end{aligned} \tag{3.32}$$

Adding Eq. (3.31) and Eq. (3.32) yields

$$\begin{aligned} &vV - vV^* + F'\left(|\psi|^2\right)\psi^2 v - F'\left(|\psi|^2\right)(\psi^2)^* v + 2\frac{d^2w}{dx^2} - 2\gamma\frac{d^4w}{dx^4} \\ &+ 2\left[-\mu + F\left(|\psi|^2\right) + F'\left(|\psi|^2\right)|\psi|^2\right]w + Vw + V^*w - F'\left(|\psi|^2\right)\psi^2 w \\ &- F'\left(|\psi|^2\right)(\psi^2)^* w = -2i\lambda v. \end{aligned} \tag{3.33}$$

Subtracting Eq. (3.32) from Eq. (3.31), we get

$$\begin{aligned} &2\frac{d^2v}{dx^2} - 2\gamma\frac{d^4v}{dx^4} + 2\left[-\mu + F\left(|\psi|^2\right) + F'\left(|\psi|^2\right)|\psi|^2\right]v + Vv + V^*v \\ &+ F'\left(|\psi|^2\right)\psi^2 v + F'\left(|\psi|^2\right)(\psi^2)^* v + Vw - V^*w - F'\left(|\psi|^2\right)\psi^2 w \\ &+ F'\left(|\psi|^2\right)(\psi^2)^* w = -2i\lambda w. \end{aligned} \tag{3.34}$$

Then, Eq. (3.33) and Eq. (3.34) are divided by 2, and the following equations are obtained, respectively

$$\begin{aligned} &\frac{1}{2}\left[V - V^* + F'\left(|\psi|^2\right)\psi^2 - F'\left(|\psi|^2\right)(\psi^2)^*\right]v + \frac{d^2w}{dx^2} - \gamma\frac{d^4w}{dx^4} \\ &+ \left[-\mu + F\left(|\psi|^2\right) + F'\left(|\psi|^2\right)|\psi|^2\right]w + \frac{1}{2}(V + V^*)w \\ &- \frac{1}{2}\left[F'\left(|\psi|^2\right)\psi^2 + F'\left(|\psi|^2\right)(\psi^2)^*\right]w = -i\lambda v, \end{aligned} \tag{3.35}$$

and

$$\begin{aligned} &\frac{d^2v}{dx^2} - \gamma\frac{d^4v}{dx^4} + \left[-\mu + F\left(|\psi|^2\right) + F'\left(|\psi|^2\right)|\psi|^2\right]v \\ &+ \frac{1}{2}(V + V^*)v + \frac{1}{2}\left[F'\left(|\psi|^2\right)\psi^2 + F'\left(|\psi|^2\right)(\psi^2)^*\right]v \\ &+ \frac{1}{2}\left[V - V^* - F'\left(|\psi|^2\right)\psi^2 + F'\left(|\psi|^2\right)(\psi^2)^*\right]w = -i\lambda w. \end{aligned} \tag{3.36}$$

Writing Eq. (3.35) and Eq. (3.36) in matrix form, we obtain the following linear stability eigenvalue problem:

$$\mathbf{L}Y = \lambda Y, \tag{3.37}$$

where

$$\mathbf{L} = i\begin{bmatrix} G_0 & \frac{d^2}{dx^2} - \gamma\frac{d^4}{dx^4} + G_1 \\ \frac{d^2}{dx^2} - \gamma\frac{d^4}{dx^4} + G_2 & G_3 \end{bmatrix}, \quad Y = \begin{bmatrix} v \\ w \end{bmatrix}, \tag{3.38}$$

and

$$
\begin{aligned}
G_0 &= iV_{im} + \frac{1}{2}\left(\psi^2 - \psi^{2^*}\right) F'\left(|\psi|^2\right), \\
G_1 &= -\mu + V_{re} + F\left(|\psi|^2\right) + \left[|\psi|^2 - \frac{1}{2}\left(\psi^2 + \psi^{2^*}\right)\right] F'\left(|\psi|^2\right), \\
G_2 &= -\mu + V_{re} + F\left(|\psi|^2\right) + \left[|\psi|^2 + \frac{1}{2}\left(\psi^2 + \psi^{2^*}\right)\right] F'\left(|\psi|^2\right), \\
G_3 &= iV_{im} - \frac{1}{2}\left(\psi^2 - \psi^{2^*}\right) F'\left(|\psi|^2\right).
\end{aligned}
\tag{3.39}
$$

For the cubic-quintic nonlinearity,

$$
\begin{aligned}
F(x) &= \alpha x + \beta x^2, \\
F'(x) &= \alpha + 2\beta x.
\end{aligned}
\tag{3.40}
$$

Inserting Eq. (3.40) in Eq. (3.39), we obtain

$$
\begin{aligned}
G_0 &= iV_{im} + \frac{1}{2}\left(\alpha + 2\beta|\psi|^2\right)\left(\psi^2 - \psi^{2^*}\right), \\
G_1 &= -\mu + V_{re} + \alpha|\psi|^2 + \beta|\psi|^4 + \left(\alpha + 2\beta|\psi|^2\right)\left[|\psi|^2 - \frac{1}{2}\left(\psi^2 + \psi^{2^*}\right)\right], \\
G_2 &= -\mu + V_{re} + \alpha|\psi|^2 + \beta|\psi|^4 + \left(\alpha + 2\beta|\psi|^2\right)\left[|\psi|^2 + \frac{1}{2}\left(\psi^2 + \psi^{2^*}\right)\right], \\
G_3 &= iV_{im} - \frac{1}{2}\left(\alpha + 2\beta|\psi|^2\right)\left(\psi^2 - \psi^{2^*}\right).
\end{aligned}
\tag{3.41}
$$

The linear-stability eigenvalue problem in Eq. (3.37) with the elements in Eq. (3.41) can be solved numerically to obtain the whole spectrum of the linear stability operator. In this thesis, we use the Fourier collocation method for this purpose, which is described in Section 2.2. If any of the calculated eigenvalues λ has a positive real part, then the soliton $\psi(x)$ is linearly unstable, otherwise, it is linearly stable. Eigenvalues of $\mathbf{L}$ always come in conjugate pairs (λ, λ^*). After the eigenvalues of the linear spectrum are calculated, it is important to determine whether these obtained eigenvalues belong to the discrete or the continuous part of the spectrum. To distinguish between these two possibilities, we examine whether the eigenfunctions associated with eigenvalues satisfy the boundary conditions, i.e. $Y \to 0$ as $|x| \to \infty$, since $\psi(x) \to 0$ and $V(x) \to 0$ as $|x| \to \infty$. If the eigenfunction satisfies the boundary conditions, we conclude that the corresponding eigenvalue belongs to the discrete spectrum. Otherwise, the eigenvalue belongs to the continuous spectrum [65]. On the other hand, if λ is in the discrete spectrum of $\mathbf{L}$, then Eq. (3.37) has nontrivial solutions $Y \in L^2$. If λ is in the continuous spectrum of $\mathbf{L}$, then Eq. (3.37) has no solution $Y \in L^2$, where $Y \neq 0$ [66]. Therefore,

the eigenvalues which belong to the continuous spectrum of linear stability operator are not eigenvalues. Consequently, we can not consider these continuum eigenvalues in linear stability analysis.

The continuous spectrum of $\mathbf{L}$ in Eq. (3.37) can be obtained from the large-distance limit of $|x| \to \infty$. Taking this limit, we have

$$\begin{aligned}
&\lim_{x\to\mp\infty} G_0 = 0, \\
&\lim_{x\to\mp\infty} \left(\frac{d^2}{dx^2} - \gamma \frac{d^4}{dx^4} + G_1 \right) = -\mu + \frac{d^2}{dx^2} - \gamma \frac{d^4}{dx^4}, \\
&\lim_{x\to\mp\infty} \left(\frac{d^2}{dx^2} - \gamma \frac{d^4}{dx^4} + G_2 \right) = -\mu + \frac{d^2}{dx^2} - \gamma \frac{d^4}{dx^4}, \\
&\lim_{x\to\mp\infty} G_3 = 0,
\end{aligned} \tag{3.42}$$

since $\lim_{x\to\mp\infty} \psi(x) = 0$ and we assume that $V(x)$ is continuous and vanishes at infinity, i.e., $V(x) \to 0$ as $|x| \to \infty$, which the potential in this thesis provides. Therefore, $\mathbf{L}$ becomes a differential operator with constant coefficients. The eigenfunction Y associated with the eigenvalue which belongs to the continuous spectrum must be a Fourier mode at large distances, which does not satisfy the boundary condition, i.e., $Y = [c_1, c_2]^T e^{ikx}$ oscillates as $|x| \to \infty$, where k is a real wavenumber, and (c_1, c_2) are constants. Therefore, the continuous spectrum of $\mathbf{L}$ is obtained by applying the large-distance limit of $\mathbf{L}$ that is given with Eq. (3.42) to $Y = [c_1, c_2]^T e^{ikx}$ as the following eigenvalue problem:

$$i \begin{bmatrix} 0 & -\mu + \dfrac{d^2}{dx^2} - \gamma \dfrac{d^4}{dx^4} \\ -\mu + \dfrac{d^2}{dx^2} - \gamma \dfrac{d^4}{dx^4} & 0 \end{bmatrix} \begin{bmatrix} c_1 e^{ikx} \\ c_2 e^{ikx} \end{bmatrix} = \lambda \begin{bmatrix} c_1 e^{ikx} \\ c_2 e^{ikx} \end{bmatrix}. \tag{3.43}$$

From Eq. (3.43), we obtain

$$\begin{aligned}
i \left(-\mu + \frac{d^2}{dx^2} - \gamma \frac{d^4}{dx^4} \right) c_2 e^{ikx} &= \lambda c_1 e^{ikx}, \\
i \left(-\mu + \frac{d^2}{dx^2} - \gamma \frac{d^4}{dx^4} \right) c_1 e^{ikx} &= \lambda c_2 e^{ikx},
\end{aligned} \tag{3.44}$$

then,

$$\begin{aligned}
i \left(-\mu + (ik)^2 - \gamma (ik)^4 \right) c_2 e^{ikx} &= \lambda c_1 e^{ikx}, \\
i \left(-\mu + (ik)^2 - \gamma (ik)^4 \right) c_1 e^{ikx} &= \lambda c_2 e^{ikx}.
\end{aligned} \tag{3.45}$$

Solving the first equation in Eq. (3.45) for c_2 and then substituting c_2 into the second equation in Eq. (3.45), we obtain

$$i\left(-\mu - k^2 - \gamma k^4\right) c_1 e^{ikx} = \lambda \frac{\lambda c_1}{i\left(-\mu - k^2 - \gamma k^4\right)} e^{ikx}. \tag{3.46}$$

Solving Eq. (3.46) for λ gives

$$\lambda = \mp i\left(\mu + k^2 + \gamma k^4\right). \tag{3.47}$$

Then, taking k to be from $-\infty$ to ∞, we find the continuous spectrum of $\mathbf{L}$ to be the two line segments $\mp i[\mu, \infty)$ on the imaginary axis.

4. SOLITONS OF CQNLS EQUATION IN $\mathcal{PT}$-SYMMETRIC POTENTIAL WITH FOURTH ORDER DISPERSION

4.1 Existence and Suppression of Symmetry-Breaking of Solitons

The continuous families of $\mathcal{PT}$-symmetric solitons are numerically obtained as solutions to the stationary Eq. (2.5) with the $\mathcal{PT}$-symmetric potential in Eq. (1.5) by using the squared-operator method explained in Section 2.1. For a better comparison, parameter values in the governing model Eq. (1.4) are chosen as $\alpha = 1$, $\beta = -0.1$, $A = 2$, $x_0 = 1.2$, and $c_0 = -0.5$, since we know that symmetry breaking of $\mathcal{PT}$-symmetric solitons occurs in cubic-quintic nonlinearity ($\gamma = 0$) with $\mathcal{PT}$-symmetric potential in Eq. (1.5) for these parameter values, when the power of the $\mathcal{PT}$-symmetric soliton crosses a certain threshold from Yang's study [49]. To examine the effect of fourth order dispersion on this symmetry breaking in the aforementioned problem, the coefficient of fourth order dispersion γ is incremented gradually from 0.1 to 1 in this study.

The potential corresponding to the above values is shown in Figure 4.1(a). The refractive index profile of the medium $V_{re}(x)$ is a double-humped function and symmetric, whereas the gain-loss distribution of the medium $V_{im}(x)$ is anti-symmetric. In addition, $g(x)$ (solid green) is a double-hump function. Its amplitude of humps is measured by A, and $\mp x_0$ are the x-values of the center of humps. Thus, the humps of the real part of this potential are also centered at $x = -x_0$ and $x = x_0$. In Figure 4.1(b)-(d), linear spectrums of the potentials with $\gamma = 0.1, \gamma = 0.41$, and $\gamma = 1$ are displayed, respectively. To obtain the linear spectrum of potential, we examine the linear eigenvalue problem in Eq. (3.37) in the absence of cubic-quintic nonlinearity by taking $\alpha = 0$ and $\beta = 0$, and $\mu = 0$. In other words, the linear eigenvalue problem which is related to the linear spectrum of the potential can be given from Eq. (2.5) for $\alpha = 0$ and $\beta = 0$

$$\mathbf{L}_V \psi = \mu \psi, \quad \mathbf{L}_V = \frac{d^2}{dx^2} - \gamma \frac{d^4}{dx^4} + V, \tag{4.1}$$

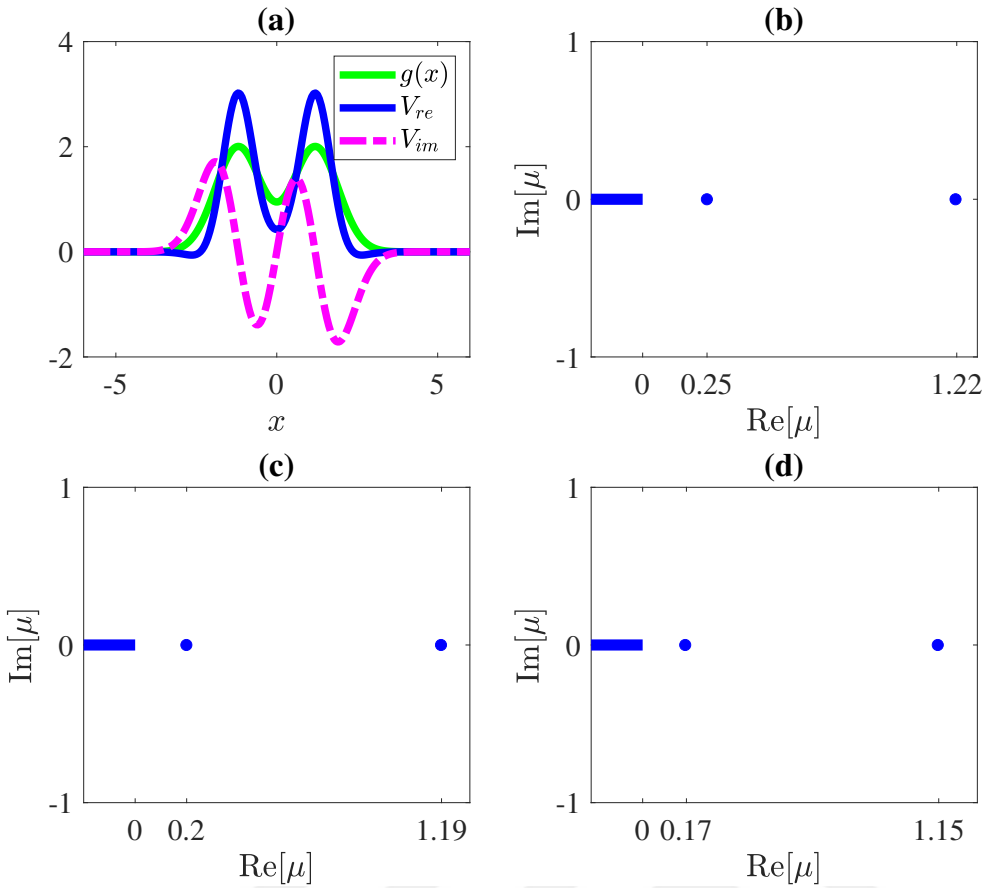

Figure 4.1 : $\mathcal{PT}$-symmetric potential given by Eqs. (1.5) and (1.6), where $A = 2$, $x_0 = 1.2$ and $c_0 = -0.5$, and its spectrum with fourth order dispersion. (a) Profile of the potential $V(x)$ [solid green, $g(x)$; solid blue, $V_{re}(x)$; dashed magenta, $V_{im}(x)$]. (b), (c) and (d) Linear spectrums of the potentials with $\gamma = 0.1$, $\gamma = 0.41$ and $\gamma = 1$, respectively.

where μ is the eigenvalue, and $\psi(x)$ is the localized eigenfunction. Although the gain-loss distribution is quite strong, each of the linear spectrums only contains two discrete real eigenvalues. For $\gamma = 0.1$, discrete real eigenvalues are

$$\mu_1 \approx 0.2495, \quad \mu_2 \approx 1.2153, \tag{4.2}$$

for $\gamma = 0.41$, we obtain discrete real eigenvalues as

$$\mu_3 \approx 0.1988, \quad \mu_4 \approx 1.1879, \tag{4.3}$$

and for $\gamma = 1$, discrete real eigenvalues are obtained as

$$\mu_5 \approx 0.1653, \quad \mu_6 \approx 1.1463. \tag{4.4}$$

Continuous families of $\mathcal{PT}$-symmetric solitons bifurcate out from the largest eigenvalues for each of $\gamma = 0.1$, $\gamma = 0.41$, and $\gamma = 1$. The power curve of

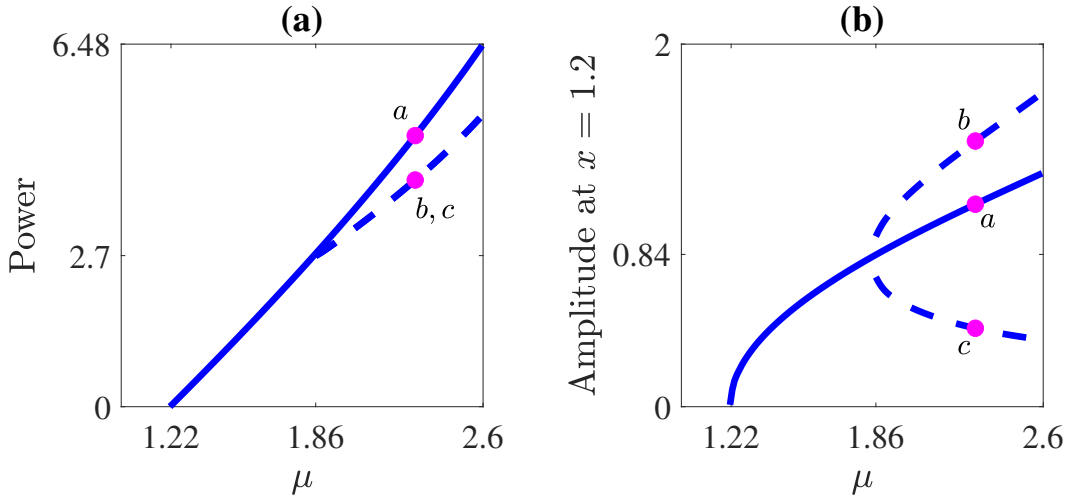

Figure 4.2 : Symmetry-breaking bifurcation of solitons in the cubic-quintic medium with fourth order dispersion $\gamma = 0.1$ and $\mathcal{PT}$-symmetric potential shown in Figure 4.1(a), where $\alpha = 1$ and $\beta = -0.1$. (a) Power of $\mathcal{PT}$-symmetric and non-$\mathcal{PT}$-symmetric (asymmetric) solitons for varying propagation constant μ, and (b) the amplitude $|\psi|$ of the soliton at the right waveguide channel $x = x_0 = 1.2$ for varying propagation constant μ. The solid blue and dashed blue curves represent the $\mathcal{PT}$-symmetric and asymmetric branches, respectively. The value of propagation constant μ at the points marked with the letters a, b, and c is 2.3 in panels (a) and (b).

the $\mathcal{PT}$-symmetric solitons and the non-$\mathcal{PT}$-symmetric (asymmetric) solitons with fourth-order dispersion $\gamma = 0.1$ are displayed in Figure 4.2(a), where the power is defined as $P(\mu) = \int_{-\infty}^{\infty} |\psi(x;\mu)|^2 dx$. As can be seen from Figure 4.2(a), this continuous family of solitons bifurcates out from $\mu > \mu_2$, and the existence region of this soliton family is obtained for $\mu \in (1.2153, 2.6]$. The $\mathcal{PT}$-symmetry of the soliton is broken with the increase of the soliton power, and the symmetry breaking occurs at $\mu_s \approx 1.86$. In other words, regardless of where the center position b_0 of the initial condition taken as a Gaussian type function in Eq. (2.54) is launched, we obtain the $\mathcal{PT}$-symmetric double-hump soliton solutions for $1.2153 < \mu < 1.86$. However, for $1.86 \leq \mu \leq 2.6$, we obtain the asymmetric solitons with energy concentrated in the left waveguide channel, the $\mathcal{PT}$-symmetric double-hump solitons, and the asymmetric solitons with energy concentrated in the right waveguide channel with initial condition launched at the center positions of $b_0 = -1.2$, $b_0 = 0$ and $b_0 = 1.2$, respectively. The $\mathcal{PT}$-symmetric and asymmetric branches are represented by the solid blue and dashed blue curves, respectively. These two asymmetric solitons have identical power curves since they are obtained as $\psi_1(x;\mu) = \psi_2^*(-x;\mu)$, which is due to the fact that the stationary Eq. (2.5) is $\mathcal{PT}$-symmetric. However, the $\mathcal{PT}$-symmetric solitons have

higher power than them. Consequently, the power curves of the $\mathcal{PT}$-symmetric and non-$\mathcal{PT}$-symmetric solitons bifurcate from the discrete linear eigenvalue $\mu_s \approx 1.86$. This bifurcation is a pitchfork-type symmetry-breaking bifurcation. In Figure 4.2(b), the amplitude $|\psi(x)|$ of the solitons at the right waveguide channel $x = x_0 = 1.2$, which is the right hump of V_{re}, is plotted for varying propagation constant μ since it is not distinguishable that the two asymmetric soliton solutions are different from each other. As can be seen from this figure, the branches of asymmetric solitons with energy concentrated in the right and left waveguide channels are above and below the base $\mathcal{PT}$-symmetric branch, respectively. Moreover, the soliton solutions at the points marked with the letters a, b, and c in this figure are obtained for the value of propagation constant $\mu = 2.3$. The soliton solution that corresponds to the point marked by the letter a is shown in Figure 4.3(a). This soliton is obtained with the initial condition launched at the center position of $b_0 = 0$. It is seen that the real part of the soliton ψ_{re} is an

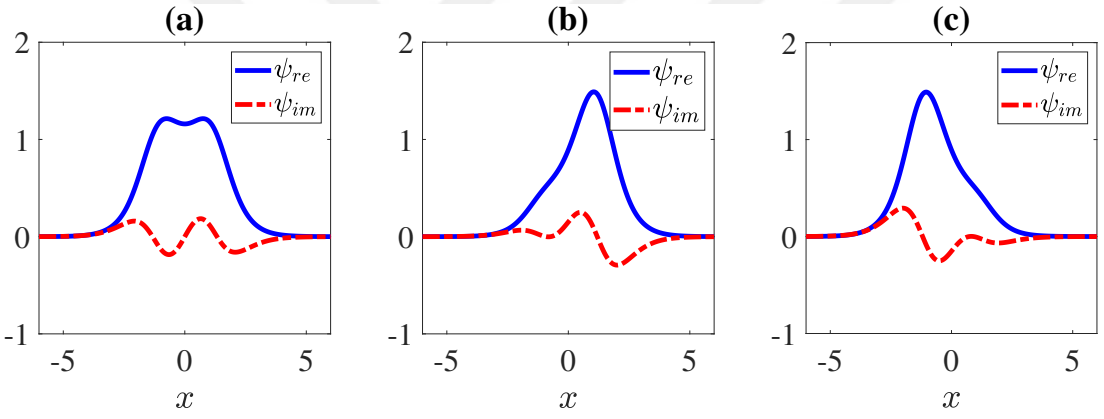

Figure 4.3 : (a) The $\mathcal{PT}$-symmetric soliton at the point marked by letter a, (b) the non-$\mathcal{PT}$-symmetric soliton at the point b, and (c) the non-$\mathcal{PT}$-symmetric soliton at the point c in Figures 4.2(a) and 4.2(b). Solid blue and dashed red curves represent the real part and the imaginary part of solitons. The value of propagation constant $\mu = 2.3$ and the coefficient of fourth order dispersion $\gamma = 0.1$

even function, and the imaginary part of the soliton ψ_{im} is an odd function because the real and imaginary parts of the soliton have reflection symmetry about the y-axis and rotational symmetry about the origin, respectively. Therefore, this soliton solution $\psi(x)$ is $\mathcal{PT}$-symmetric. In Figures 4.3(b) and 4.3(c), the non-$\mathcal{PT}$-symmetric solitons at points marked by letters b and c in Figure 4.2 are displayed. If the center position of the initial condition is chosen as $b_0 = 1.2$, the non-$\mathcal{PT}$-symmetric soliton with energy concentrated in the right waveguide channel in Figure 4.3(b) is obtained. The soliton in

Figure 4.3(c) is obtained by taking the initial condition with center position $b = -1.2$. It is seen that most of the energy in these non-$\mathcal{PT}$-symmetric solitons in Figures 4.3(b) and 4.3(c) resides on the right and left sides of the potential, respectively. The real and imaginary parts of these non-$\mathcal{PT}$-symmetric solitons are asymmetric. From Figures 4.3(b) and 4.3(c), it can be seen that these two non-$\mathcal{PT}$-symmetric solitons are related by $\psi_1(x) = \psi_2^*(-x)$, which confirms the above statement that their powers are equal.

The $\mathcal{PT}$-symmetry-breaking bifurcation of solitons occurs for the coefficient of fourth order dispersion $0 \leq \gamma < 0.41$. Nevertheless, the results we have obtained show that the $\mathcal{PT}$-symmetry-breaking bifurcation can be intensely influenced by the strength of the fourth order dispersion. We observe that the symmetry breaking is completely suppressed when the coefficient of fourth order dispersion is taken as $\gamma = 0.41$. In other words, no matter what we take the center position b_0 of the initial condition, a $\mathcal{PT}$-symmetric soliton is always obtained. Moreover, the shapes of these solitons also change, and they have a single-hump rather than a double-hump. In Figure 4.4(a), the

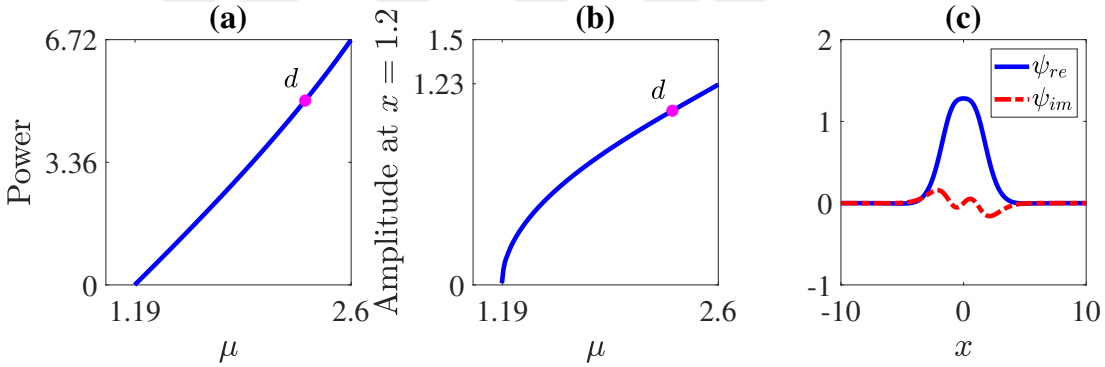

Figure 4.4 : Suppression of $\mathcal{PT}$-symmetry-breaking bifurcation of solitons in the cubic-quintic medium with fourth order dispersion $\gamma = 0.41$ in $\mathcal{PT}$-symmetric potential shown in Figure 4.1(a), where $\alpha = 1$ and $\beta = -0.1$. (a) Power curve of $\mathcal{PT}$-symmetric single-hump solitons for varying propagation constant μ, and (b) the amplitude $|\psi|$ of the soliton at the right waveguide channel $x = x_0 = 1.2$ for varying propagation constant μ. In panels (a) and (b), the value of propagation constant μ at the point marked with the letter d is 2.3. (c) The real (solid blue) and imaginary (dashed red) parts of soliton at point d.

power curve of this single-hump soliton family is displayed. As can be seen from this power curve, these $\mathcal{PT}$-symmetric single-hump solitons bifurcate out from the largest eigenvalue $\mu_4 \approx 1.1879$ of the linear spectrum of potential with fourth order dispersion $\gamma = 0.41$. Furthermore, the existence region of this $\mathcal{PT}$-symmetric single-hump

solitons is obtained as for $\mu \in (1.1879, 2.6]$. In Figure 4.4(b), the amplitude $|\psi|$ of the single-hump soliton at the right waveguide channel $x = x_0 = 1.2$ is shown for varying propagation constant μ. The point d which is marked in Figures 4.4(a) and 4.4(b) is related to the single-hump soliton for $\mu = 2.3$. This single-hump soliton that corresponds to the point d is shown in Figure 4.4(c). The real part of this single-hump soliton is even whereas its imaginary part is odd. Thus, this soliton is $\mathcal{PT}$-symmetric.

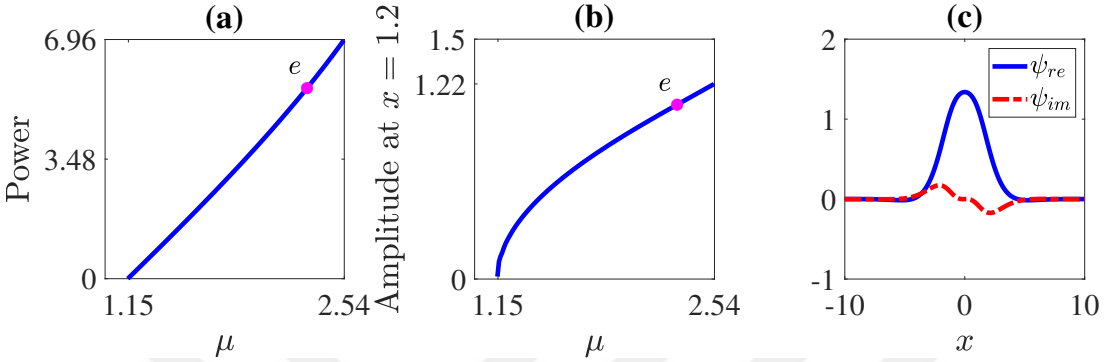

Figure 4.5 : The $\mathcal{PT}$-symmetric single-hump solitons in the cubic-quintic medium with fourth order dispersion $\gamma = 1$ in $\mathcal{PT}$-symmetric potential shown in Figure 4.1(a), where $\alpha = 1$ and $\beta = -0.1$. (a) Power curve of $\mathcal{PT}$-symmetric single-hump solitons for varying propagation constant μ, and (b) the amplitude $|\psi|$ of the soliton at the right waveguide channel $x = x_0 = 1.2$ for varying propagation constant μ. In panels (a) and (b), the value of propagation constant μ at the point marked with the letter e is 2.3. (c) The real (solid blue) and imaginary (dashed red) parts of soliton at point e.

The strength of fourth-order dispersion is incremented gradually to check whether the suppression of symmetry breaking is preserved. We have observed that symmetry breaking continues to be suppressed for the stronger coefficient of fourth-order dispersion as well. As an example, the results obtained for $\gamma = 1$ are given in Figure 4.5. As can be seen from this figure, there is a single power curve because we get the same $\mathcal{PT}$-symmetric single-hump soliton no matter what we take as the center position b_0 of the initial condition. Consequently, the $\mathcal{PT}$-symmetry-breaking of solitons is also completely suppressed for $\gamma = 1$. Similarly, it can be seen from Figure 4.5(a) that these solitons bifurcate out from the largest eigenvalue $\mu_6 \approx 1.1463$ of the linear spectrum of potential with fourth order dispersion $\gamma = 1$. The power curve and amplitude (at the right waveguide channel) of this soliton family are shown in Figures 4.5(a) and 4.5(b), respectively. The profile of the $\mathcal{PT}$-symmetric single-hump soliton at the point marked by the letter e in Figures 4.5(a) and 4.5(b) is shown in Figure 4.5(c).

4.2 Stability Analysis of $\mathcal{PT}$-Symmetric and Non-$\mathcal{PT}$-Symmetric Solitons

4.2.1 Nonlinear stability

If a soliton preserves its shape, location, and maximum amplitude during nonlinear evolution, it is considered nonlinearly stable. The nonlinear stability of the obtained solitons is examined by nonlinear evolution simulations of these solitons by using the split-step Fourier method (see Section 3.1).

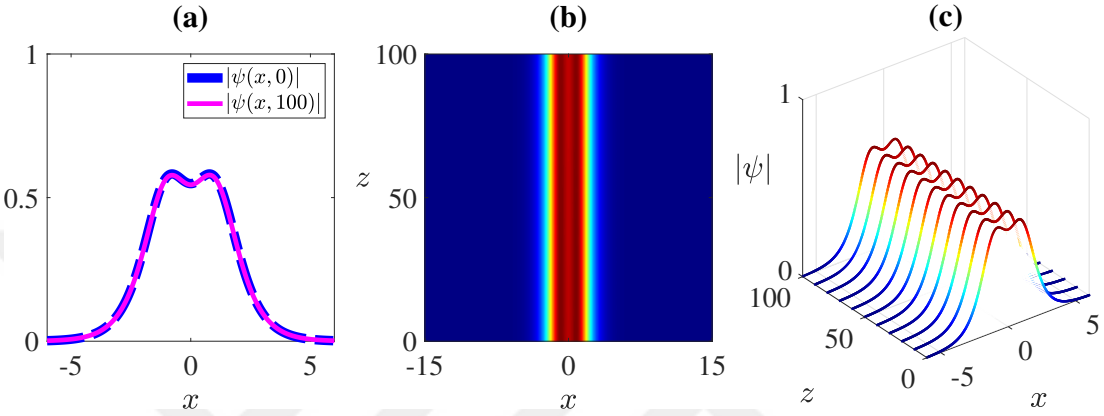

Figure 4.6 : Nonlinear evolution of the $\mathcal{PT}$-symmetric double-hump soliton in the cubic-quintic ($\alpha = 1$, $\beta = -0.1$) medium with fourth order dispersion $\gamma = 0.1$ and $\mathcal{PT}$-symmetric potential shown in Figure 4.1(a) for $\mu = 1.5$ which is before the symmetry-breaking bifurcation point. (a) Profile of numerically obtained soliton (dashed blue) and its profile at the propagation distance $z = 100$ (solid magenta), (b) View of nonlinear evolution of soliton from the top, (c) Three dimensional plot depicting this evolution.

Firstly, we have examined the nonlinear stability of solitons on the $\mathcal{PT}$-symmetric branch of Figure 4.2(b) before the symmetry-breaking bifurcation point $\mu_s \approx 1.86$, where we have obtained that symmetry breaking occurs for fourth order dispersion $\gamma = 0.1$. Nonlinear stability analysis of $\mathcal{PT}$-symmetric double-hump soliton which is obtained for $\mu = 1.5$ can be shown in Figure 4.6. Profile of soliton $|\psi(x,0)|$ obtained by using SOM and its profile $|\psi(x,100)|$ at the propagation distance $z = 100$ are respectively plotted as dashed blue and solid magenta curves in Figure 4.6(a). Maximum amplitudes of profiles $|\psi(x,0)|$ and $|\psi(x,100)|$ are approximately 0.582 and 0.579, respectively. This variation in amplitude during evolution can be negligible, and this soliton is considered nonlinearly stable. From Figures 4.6(b) and 4.6(c), it can be seen that the soliton conserves also its shape and location during its evolution.

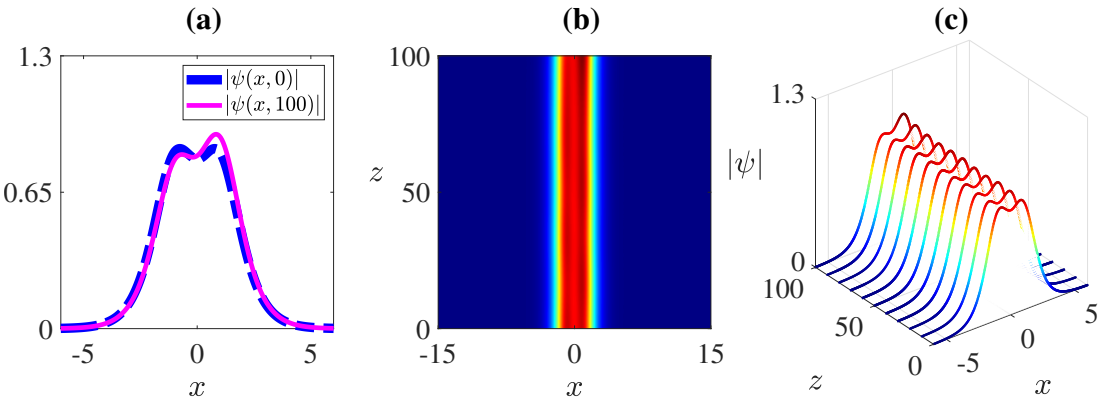

Figure 4.7 : Nonlinear evolution of the $\mathcal{PT}$-symmetric double-hump soliton in cubic-quintic ($\alpha = 1$, $\beta = -0.1$) medium with fourth order dispersion $\gamma = 0.1$ and $\mathcal{PT}$-symmetric potential shown in Figure 4.1(a) for $\mu = 1.8$ which is before the symmetry-breaking bifurcation point. (a) Profile of numerically obtained soliton (dashed blue) and its profile at the propagation distance $z = 100$ (solid magenta), (b) View of nonlinear evolution of soliton from the top, (c) Three dimensional plot depicting this evolution.

Solitons become nonlinearly unstable as the propagation constant approaches the symmetry-breaking bifurcation point $\mu_s \approx 1.86$, which has been observed to occur for $\mu \geq 1.8$. In Figure 4.7, the results of the nonlinear stability analysis are given for $\mu = 1.8$. Although this $\mathcal{PT}$-symmetric double-hump soliton seems nonlinearly stable at the beginning of evolution, it is noticed that the amplitude of the left-hump decrease while the amplitude of the right-hump increase. In other words, it is easily seen that this $\mathcal{PT}$-symmetric double-hump soliton becomes non-$\mathcal{PT}$-symmetric (asymmetric) at the end of evolution. Therefore, it is nonlinearly unstable. Then, we have examined the nonlinear evolutions of solitons in Figure 4.3, which are obtained after the symmetry-breaking bifurcation point, i.e., for propagation constant $\mu = 2.3 > \mu_s$. The stability analysis of $\mathcal{PT}$-symmetric double-hump soliton in Figure 4.3(a) is displayed in Figure 4.8. As can be seen from this figure, the $\mathcal{PT}$-symmetric double-hump soliton can propagate nonlinearly stable over a short distance then the energy of the double-hump soliton is concentrated in the right waveguide channel. Hence, it becomes non-$\mathcal{PT}$-symmetric. Afterward, its energy is concentrated in the left waveguide channel, and the amplitude of soliton oscillates as the evolution continues. Consequently, this $\mathcal{PT}$-symmetric double-hump soliton is not nonlinearly stable. The results of the nonlinear evolution in Figure 4.9 indicate that the non-$\mathcal{PT}$-symmetric soliton in Figure 4.3(b) is nonlinearly unstable since its amplitude firstly increases

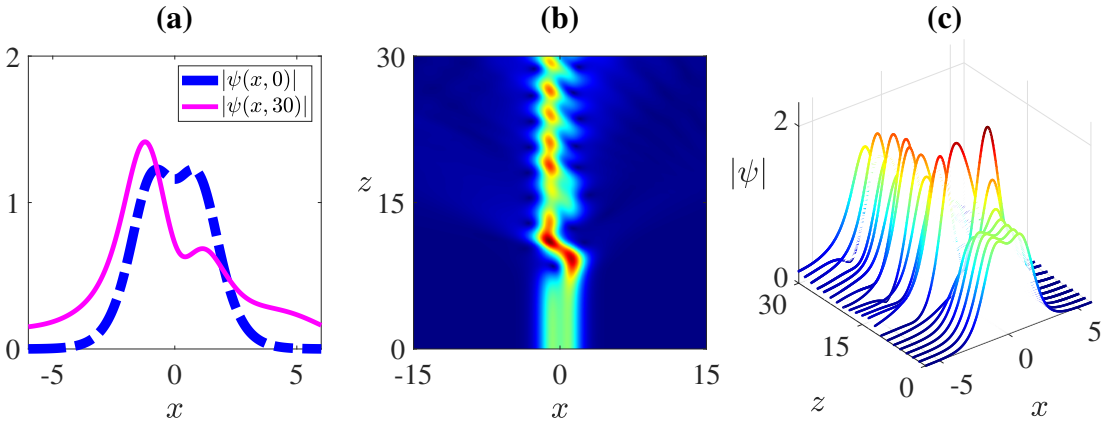

Figure 4.8 : Nonlinear evolution of the $\mathcal{PT}$-symmetric double-hump soliton in Figure 4.3(a) (for $\gamma = 0.1, \mu = 2.3$, and $b_0 = 0$). (a) Profile of numerically obtained soliton (dashed blue) and its profile at the propagation distance $z = 30$ (solid magenta), (b) View of nonlinear evolution of soliton from the top, (c) Three dimensional plot depicting this evolution.

during evolution, then its energy is concentrated in the left waveguide channel, and it continues to propagate by oscillating. In Figure 4.10, the nonlinear stability analysis of the non-$\mathcal{PT}$-symmetric soliton with energy concentrated in the left waveguide channel (in Figure 4.3(c)) is demonstrated. During the nonlinear evolution, the amplitude of this soliton decreases, and then it moves to the right waveguide channel. Afterward, its amplitude begins to increase again. As can be seen from the figure, after this soliton moves to the right waveguide channel, the evolution continues similar to the evolution of the non-$\mathcal{PT}$-symmetric soliton with energy concentrated in the right waveguide

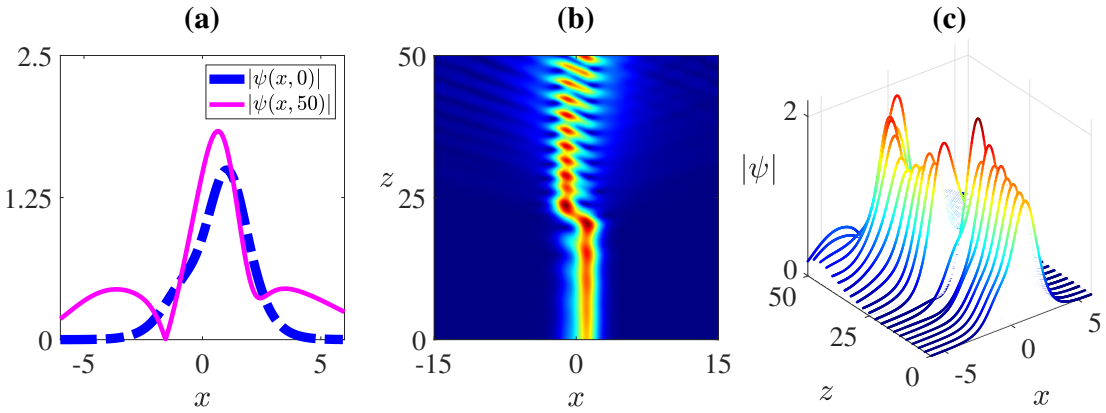

Figure 4.9 : Nonlinear evolution of the non-$\mathcal{PT}$-symmetric soliton in Figure 4.3(b) (for $\gamma = 0.1, \mu = 2.3$, and $b_0 = 1.2$). (a) Profile of numerically obtained soliton (dashed blue) and its profile at the propagation distance $z = 50$ (solid magenta), (b) View of nonlinear evolution of soliton from the top, (c) Three dimensional plot depicting this evolution.

channel (see Figure 4.9). It is noticed that these two non-$\mathcal{PT}$-symmetric solitons in a symmetry-breaking bifurcation have the same evolution dynamics. As a result, this non-$\mathcal{PT}$-symmetric soliton is also nonlinearly unstable.

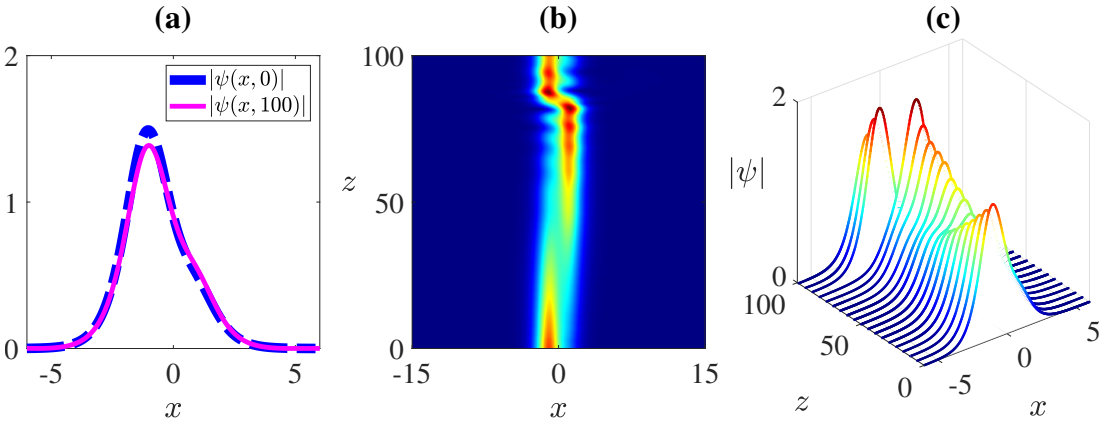

Figure 4.10 : Nonlinear evolution of the non-$\mathcal{PT}$-symmetric soliton in Figure 4.3(c) (for $\gamma = 0.1, \mu = 2.3$, and $b_0 = -1.2$). (a) Profile of numerically obtained soliton (dashed blue) and its profile at the propagation distance $z = 100$ (solid magenta), (b) View of nonlinear evolution of soliton from the top, (c) Three dimensional plot depicting this evolution.

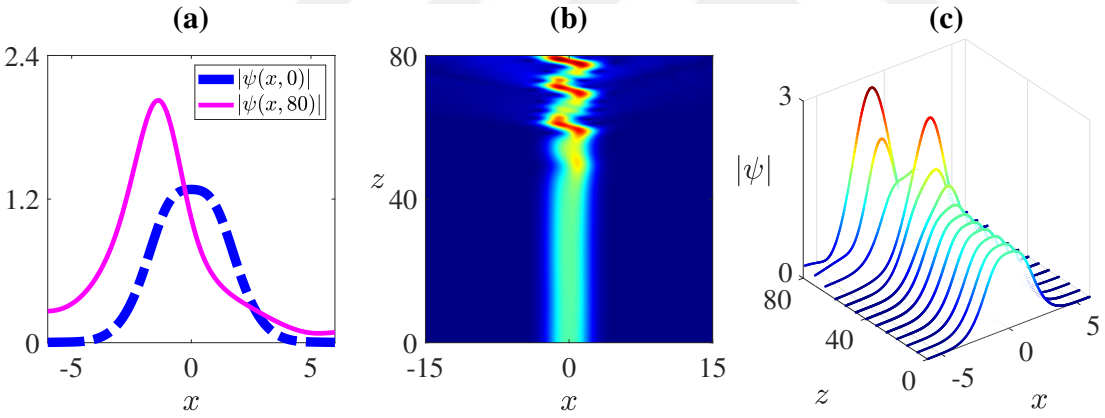

Figure 4.11 : Nonlinear stability of the $\mathcal{PT}$-symmetric single-hump soliton in Figure 4.4(c) (for $\gamma = 0.41$, and $\mu = 2.3$). (a) Profile of numerically obtained soliton (dashed blue) and its profile at the propagation distance $z = 80$ (solid magenta), (b) View of nonlinear evolution of soliton from the top, (c) Three dimensional plot depicting this evolution.

To examine the nonlinear stability of solitons obtained when the symmetry-breaking bifurcation is suppressed, we first consider the evolution of the $\mathcal{PT}$-symmetric single-hump soliton in cubic-quintic ($\alpha = 1, \beta = -0.1$) medium with fourth order dispersion $\gamma = 0.41$ at the same propagation constant $\mu = 2.3$ for a better comparison, which is the soliton shown in Figure 4.4(c). The nonlinear stability analysis of this

soliton is given in Figure 4.11. Even if this soliton cannot be assumed as nonlinearly stable since its energy oscillates between the left and right waveguide channels (i.e., between two humps of the potential), it can be seen that this soliton propagates nonlinearly stable over a longer propagation distance z than the above solitons. Moreover, we examine the nonlinear evolution of the $\mathcal{PT}$-symmetric single-hump soliton obtained for propagation constant $\mu = 2.3$ with fourth order dispersion $\gamma = 1$ in which the symmetry-breaking bifurcation has been suppressed (see Figure 4.5). The evolution of the corresponding soliton is depicted in Figure 4.12. This figure reveals that this $\mathcal{PT}$-symmetric single-hump soliton is nonlinearly stable since it preserves its shape, location, and maximum amplitude for a long distance. Thus, we have demonstrated that the stability of solitons can be improved by increasing the coefficient of fourth order dispersion. Consequently, it is concluded that the fourth order dispersion has a positive effect on the nonlinear stability of solitons in addition to suppressing symmetry-breaking bifurcation.

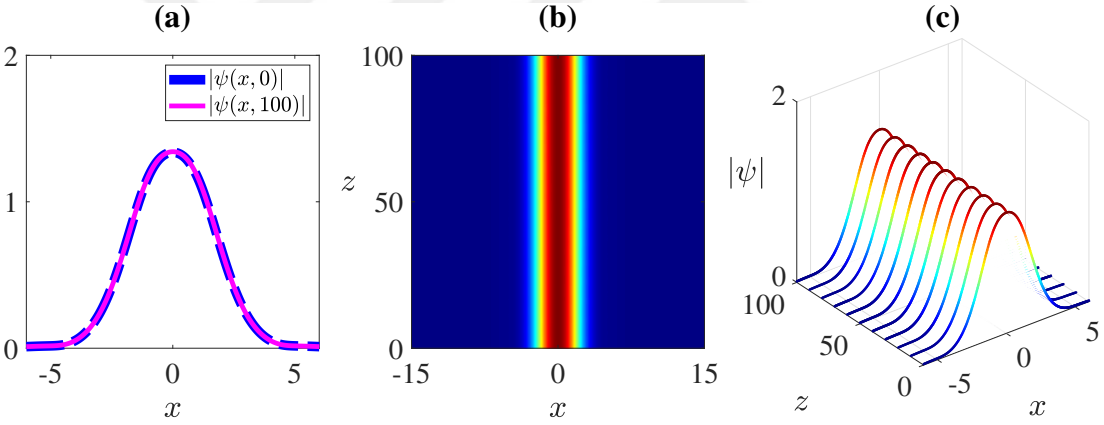

Figure 4.12 : Nonlinear stability of the $\mathcal{PT}$-symmetric single-hump soliton in Figure 4.5(c) (for $\gamma = 1$, and $\mu = 2.3$). (a) Profile of numerically obtained soliton (dashed blue) and its profile at the propagation distance $z = 100$ (solid magenta), (b) View of nonlinear evolution of soliton from the top, (c) Three dimensional plot depicting this evolution.

4.2.2 Linear stability

In this subsection, we have analyzed the linear stability of the $\mathcal{PT}$-symmetric and asymmetric solitons. To compute the whole spectrum of the linear stability eigenvalue problem in Eq. (3.37), we use the Fourier collocation method which is explained in Section 2.2. In summary, we again would like to emphasize that if any of the

calculated eigenvalues λ has a positive real part, then the soliton $\psi(x)$ is linearly unstable, otherwise, it is linearly stable.

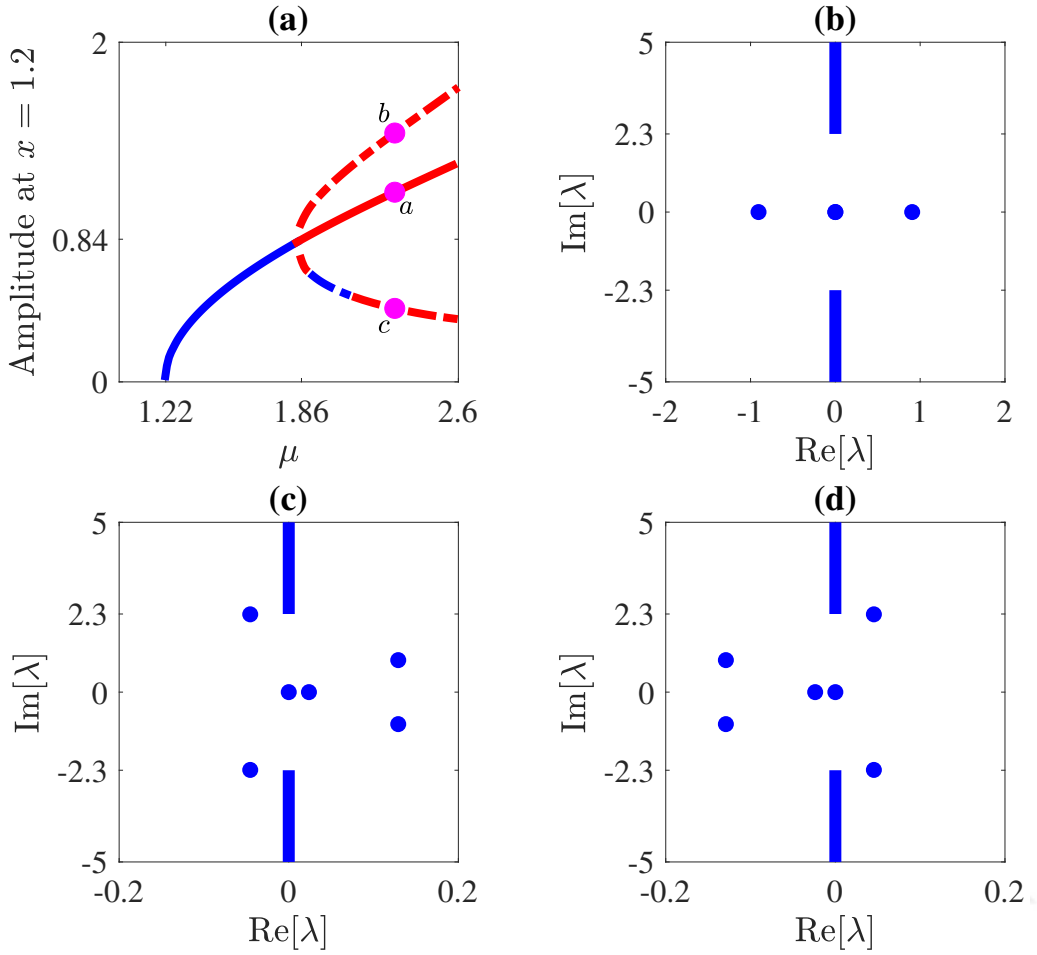

Figure 4.13 : The linear stability results of the linear eigenvalue problem in Eq. (3.37) for the fourth order dispersion $\gamma = 0.1$. (a) Copy of Figure 4.2(b) with linear stability dynamic. Blue curves for linearly stable and red curves for linearly unstable. The linear-stability eigenvalue spectrums of (b) the $\mathcal{PT}$-symmetric double-hump soliton at the point a, (c) the asymmetric soliton at the point b, and (d) the asymmetric soliton at the point c (also see Figure 4.3 for the profiles of these solitons). The value of propagation constant μ at these points marked with the letters a, b, c is 2.3

In Figure 4.13, the linear stability results of the linear eigenvalue problem in Eq. (3.37) for the fourth order dispersion $\gamma = 0.1$ are given. As can be seen, the panel (a) in Figure 4.13 is a copy of Figure 4.2(b), but also includes the corresponding linear stability results. Blue curves (solid or dashed) are used to indicate linearly stable intervals of the propagation constant, while red curves (solid or dashed) indicate linearly unstable intervals. As can be seen from Figure 4.13(a), for the fourth order dispersion $\gamma = 0.1$, in which case the symmetry-breaking occurs, the $\mathcal{PT}$-symmetric branch of

solitons is linearly stable when $\mu \in (1.2153, 1.8214)$, since the corresponding linear spectrums contain a pair of discrete eigenvalues on the imaginary axis in addition to zero eigenvalues. It is seen that the $\mathcal{PT}$-symmetric solitons become unstable as the propagation constant μ approaches the symmetry-breaking point $\mu_s \approx 1.86$. The pair of purely imaginary eigenvalues moves to the origin and collides there, at $\mu \approx 1.8214$. For $\mu > 1.8214$ and as well as after symmetry-breaking bifurcation, these pair of eigenvalues bifurcates off along the real axis. Therefore, the $\mathcal{PT}$-symmetric branch becomes linearly unstable for $\mu > 1.8214$. The upper non-$\mathcal{PT}$-symmetric branch corresponding to asymmetric solitons with energy concentrated in the right waveguide channel is linearly unstable due to the appearance of a positive real eigenvalue. In addition to the positive real eigenvalue, for $\mu > 1.8945$, the conjugate pair of eigenvalues on the left half of the complex plane shift to the right half of the complex plane, and become unstable. Moreover, for $\mu \geq 2.1$, a conjugate pair of discrete eigenvalues bifurcates out from the edges of the continuous spectrum, i.e., at the points $\lambda = \mp i\mu$, and moves to the left half of the complex plane as μ increases. The lower non-$\mathcal{PT}$-symmetric branch corresponding to asymmetric solitons with energy concentrated in the left waveguide channel is linearly stable for $\mu \in [1.8945, 2.1)$ and linearly unstable for $\mu \in [1.86, 1.8945) \cup [2.1, 2.6]$. In addition to zero eigenvalues and a negative real eigenvalue, the corresponding linear spectrum has a conjugate pair of discrete eigenvalues on the right half of the complex plane, which are unstable eigenvalues, for $\mu \in [1.86, 1.8945)$. Then, at $\mu = 1.8945$, the conjugate pair of discrete eigenvalues is on the imaginary axis, and for $\mu > 1.8945$, they move to the stable region of the imaginary plane. Therefore, they become stable eigenvalues. However, at $\mu = 2.1$, a conjugate pair of discrete eigenvalues emerge from the edges of the continuous spectrum. Moreover, they move to the right as the propagation constant μ of the soliton increases in $[2.1, 2.6]$. Consequently, although the lower branch becomes linearly stable at $\mu = 1.8945$, it becomes linearly unstable again for $\mu \in [2.1, 2.6]$. It should be noted that the movements and bifurcations of the eigenvalues, which occur as the propagation constant μ varies, are symmetric for the upper and lower asymmetric branches at the identical value of μ. Then, we have plotted the linear-stability eigenvalue spectrums of the $\mathcal{PT}$-symmetric double-hump soliton at the point a, the asymmetric soliton with energy concentrated in the right

waveguide channel at the point b, and the asymmetric soliton with energy concentrated in the left waveguide channel at the point c in Figures 4.13(b), 4.13(c), and 4.13(d), respectively. The profiles of these solitons can be seen in Figure 4.3. As shown in Figure 4.13(b), the $\mathcal{PT}$-symmetric double-hump soliton is linearly unstable due to the presence of a pair of discrete real eigenvalues, one of which is positive. Figure 4.13(c) indicates that the spectrum of the non-$\mathcal{PT}$-symmetric soliton with energy concentrated in the right waveguide channel at the point b has a positive real eigenvalue and a pair of conjugate discrete eigenvalues on the right half of the complex plane in addition to zero eigenvalues and a bifurcating pair of eigenvalues. Therefore, it is linearly unstable. The asymmetric soliton whose energy is concentrated in the left waveguide

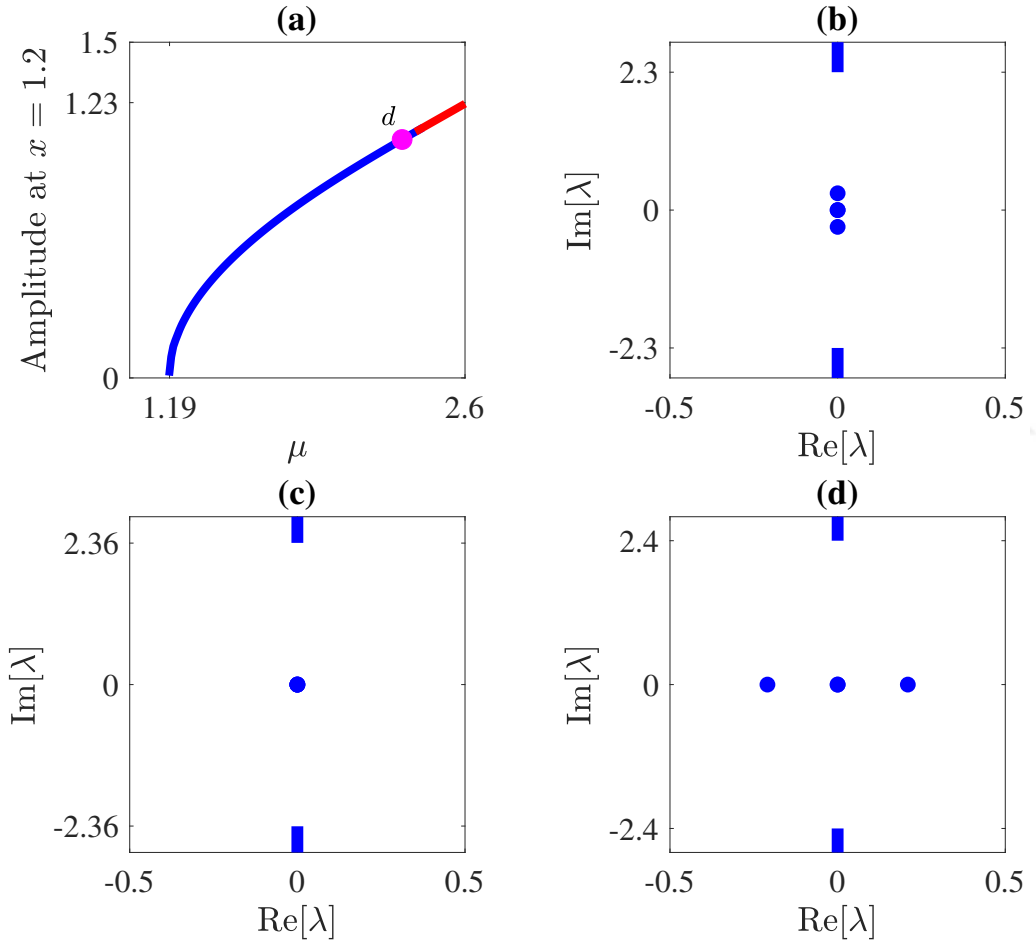

Figure 4.14 : The linear stability results of the linear eigenvalue problem in Eq. (3.37) for the fourth order dispersion $\gamma = 0.41$. (a) Copy of Figure 4.4(b) with linear stability dynamic. Blue curve for linearly stable and red curve for linearly unstable. The linear-stability eigenvalue spectrums of the $\mathcal{PT}$-symmetric single-hump solitons (b) at the point d which is for the propagation constant $\mu = 2.3$ (also see Figure 4.4(c) for the profile of this soliton), (c) for the propagation constant $\mu = 2.3638$, and (d) for the propagation constant $\mu = 2.4$.

channel at the point c is also linearly unstable since its linear spectrum contains a pair of eigenvalues bifurcating from the edges of the continuous spectrum, which are on the right half of the complex plane (the unstable region). Moreover, the eigenvalues in the spectrum of the asymmetric soliton with the energy concentrated in the right waveguide channel are negatives of the eigenvalues in the spectrum of the asymmetric soliton with the energy concentrated in the left waveguide channel. This is because these two asymmetric solitons are related as $\psi_1(x) = \psi_2^*(-x)$, it can be seen in Figures 4.3(b) and 4.3(c).

Figure 4.14 demonstrates the linear stability results of the linear eigenvalue problem in Eq. (3.37) for the fourth order dispersion $\gamma = 0.41$. The single-hump solitons on this

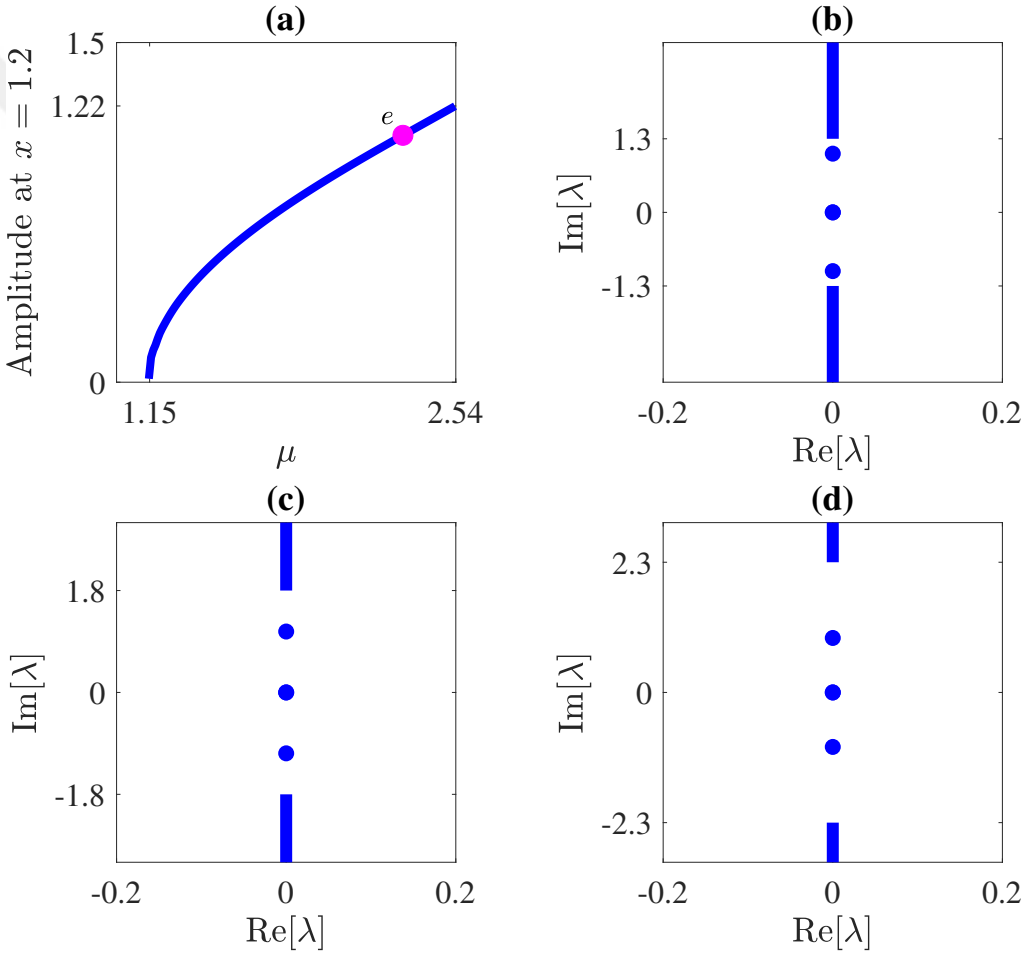

Figure 4.15 : The linear stability results of the linear eigenvalue problem in Eq. (3.37) for the fourth order dispersion $\gamma = 1$. (a) Copy of Figure 4.5(b) with linear stability dynamic. Blue curve represents linearly stable. The linear-stability eigenvalue spectrums of the $\mathcal{PT}$-symmetric single-hump solitons (b) for the propagation constant $\mu = 1.3$, (c) for the propagation constant $\mu = 1.8$, and (d) at the point e which is for the propagation constant $\mu = 2.3$ (also see Figure 4.5(c) for the profile of this soliton).

$\mathcal{PT}$-symmetric branch are obtained as linearly stable for the propagation constant $\mu \in (1.1879, 2.3638]$, whereas they are obtained as linearly unstable for the propagation constant $\mu \in (2.3638, 2.6]$. To better understand how these solitons become linearly unstable, in Figures 4.14(b)-4.14(d), we have plotted the linear spectrums of solitons for certain values of the propagation constant, which are $\mu = 2.3$, $\mu = 2.3638$, and $\mu = 2.4$, respectively. As can be seen from this figure, the soliton obtained for $\mu = 2.3$ is linearly stable, since its spectrum contains a conjugate pair of discrete eigenvalues on the imaginary axis in addition to zero eigenvalues. We observe that this conjugate pair of eigenvalues moves to the origin as μ increases. For $\mu = 2.3638$, they merge at the origin and then bifurcate off along the real axis. Therefore, these solitons become linearly unstable after this value of μ.

In Figure 4.15, the results of linear stability analysis are displayed for the fourth order dispersion $\gamma = 1$. The results reveal that all of the $\mathcal{PT}$-symmetric single-hump solitons in cubic-quintic ($\alpha = 1$ and $\beta = -0.1$) medium with fourth order dispersion $\gamma = 1$ in $\mathcal{PT}$-symmetric potential shown in Figure 4.1(a) are linearly stable. In Figures 4.15(b)-4.15(d), the linear spectrums of solitons for the propagation constants $\mu = 1.3$, $\mu = 1.8$, and $\mu = 2.3$ are shown, respectively. It can be seen that all these spectrums have a conjugate pair of purely imaginary eigenvalues in addition to zero eigenvalues. Therefore, they are linearly stable. Consequently, increasing the strength of the fourth order dispersion positively influences the linear stability of solitons.

5. CONCLUSIONS AND RECOMMENDATIONS

In this thesis, the existence of symmetry breaking of optical solitons and the suppression of symmetry-breaking bifurcations have been numerically investigated in cubic-quintic medium with the fourth order dispersion and special $\mathcal{PT}$-symmetric potential. Thus, the governing equation is the CQNLS equation added fourth order dispersion and $\mathcal{PT}$-symmetric potential.

Firstly, we compute the spectrum of $\mathcal{PT}$-symmetric potential with various strengths of fourth order dispersion. Then, we have numerically obtained the soliton solutions by using the squared-operator method and it is noticed that the continuous families of $\mathcal{PT}$-symmetric solitons bifurcate out from the largest discrete eigenvalue of the associated spectrum. We have found that two branches of non-$\mathcal{PT}$-symmetric solitons bifurcate from the base branch of $\mathcal{PT}$-symmetric solitons by a pitchfork bifurcation when the base branch's power crosses a specific threshold for the weak fourth order dispersion. Nevertheless, the results we have obtained show that the $\mathcal{PT}$-symmetry-breaking bifurcation is completely suppressed by increasing the strength of fourth order dispersion. Moreover, the shapes of solitons also change as a single hump.

To examine the nonlinear stability of the numerically obtained $\mathcal{PT}$-symmetric and non-$\mathcal{PT}$-symmetric solitons, their nonlinear evolution simulations in long-distance propagation have been investigated by employing the split-step Fourier method. We first have examined in case of symmetry breaking of solitons. On the $\mathcal{PT}$-symmetric branch before the bifurcation point, double-hump solitons are found as nonlinearly stable. However, they become nonlinearly unstable as the propagation constant exceeds a specific value that is near the symmetry-breaking bifurcation point. In addition, after the symmetry-breaking bifurcation point, we have demonstrated that the $\mathcal{PT}$-symmetric and non-$\mathcal{PT}$-symmetric solitons are nonlinearly unstable. Then, the nonlinear stability dynamics of solitons that are obtained when the symmetry breaking is suppressed by higher strength of fourth order dispersion have been investigated.

We have observed that increasing the coefficient of fourth-order dispersion extends the propagation distance in which solitons are nonlinearly stable. Furthermore, they become completely nonlinearly stable after a certain strength of fourth order dispersion.

We also have analyzed the linear stability of solitons by computing the whole spectrum of their linear stability operator. When the $\mathcal{PT}$-symmetric solitons undergo symmetry breaking, their linear stability results have shown that solitons become linearly unstable as the propagation constant approaches the bifurcation point. After the bifurcation point, the branches of $\mathcal{PT}$-symmetric solitons and asymmetric solitons with energy concentrated in the right waveguide channel are not linearly stable. The asymmetric solitons with energy concentrated in the left waveguide channel are first linearly unstable, then they become stable in a certain interval of the propagation constant. However, they become linearly unstable again since a conjugate pair of discrete eigenvalues bifurcates out from the edges of the continuous spectrum and moves to the unstable half of the complex plane as the propagation constant increases. By increasing the strength of fourth order dispersion, the linear spectrum of obtained solitons has only a conjugate pair of purely imaginary eigenvalues in addition to zero eigenvalues. Therefore, they are obtained as linearly stable.

In summary, it is important to note that the symmetry-breaking bifurcation of $\mathcal{PT}$-symmetric solitons is completely suppressed by increasing the strength of fourth order dispersion. Moreover, we have concluded that the fourth order dispersion positively influences the linear and nonlinear stability of solitons.

As a future study, we recommend that this study can be extended for the existence and suppression of symmetry-breaking bifurcations of (2+1)D solitons in a $\mathcal{PT}$-symmetric system with higher-order dispersion effects.

REFERENCES

[1] **Lomdahl, P.S.** (1984). What is a soliton. *Los Alamos Science*, *10*, 27–31.

[2] **Ablowitz, M.J.** (2011). *Nonlinear dispersive waves: asymptotic analysis and solitons* (Vol. 47). Cambridge University Press.

[3] **Sulem, C. and Sulem, P.L.** (2007). *The nonlinear Schrödinger equation: self-focusing and wave collapse* (Vol.139). Springer Science & Business Media.

[4] **Stegeman, G.I.**, **Christodoulides, D.N. and Segev, M.** (2000). Optical spatial solitons: historical perspectives. *IEEE Journal of Selected Topics in Quantum Electronics*, *6*(6), 1419–1427.

[5] **Kivshar, Y.S. and Agrawal, G.P.** (2003). *Optical Solitons: from fibers to photonic crystals*. Academic Press.

[6] **Hasegawa, A. and Tappert, F.** (1973). Transmission of stationary nonlinear optical pulses in dispersive dielectric fibers. I. Anomalous dispersion. *Applied Physics Letters*, *23*(3), 142–144.

[7] **Hasegawa, A. and Tappert, F.** (1973). Transmission of stationary nonlinear optical pulses in dispersive dielectric fibers. II. Normal dispersion. *Applied Physics Letters*, *23*(4), 171–172.

[8] **Mollenauer, L.F.**, **Stolen, R.H. and Gordon, J.P.** (1980). Experimental observation of picosecond pulse narrowing and solitons in optical fibers. *Physical Review Letters*, *45*(13), 1095.

[9] **Kapron, F.P.** (1977). Maximum information capacity of fibre-optic waveguides. *Electronics Letters*, *4*(13), 96–97.

[10] **Kohl, R.**, **Biswas, A.**, **Milovic, D. and Zerrad, E.** (2008). Optical soliton perturbation in a non-Kerr law media. *Optics & Laser Technology*, *40*(4), 647–662.

[11] **Karlsson, M. and Höök, A.** (1994). Soliton-like pulses governed by fourth order dispersion in optical fibers. *Optics Communications*, *104*(4-6), 303–307.

[12] **Agrawal, G.P.** (2013). *Nonlinear Fiber Optics*. (Fifth Edition), Academic Press.

[13] **Zakharov, V.E.** (1972). Collapse of Langmuir waves. *Sov. Phys. JETP*, *35*(5), 908–914.

[14] **Yang, J.** (2010). *Nonlinear waves in integrable and nonintegrable systems*, Society for Industrial and Applied Mathematics.

[15] **Ablowitz, M.J.**, **Antar, N.**, **Bakırtaş, İ. and Ilan, B.** (2010). Band-gap boundaries and fundamental solitons in complex two-dimensional nonlinear lattices. *Physical Review A*, *81*(3), 033834.

[16] **Bağcı, M.**, **Bakırtaş, İ. and Antar, N.** (2014). Vortex and dipole solitons in lattices possessing defects and dislocations. *Optics Communications*, *331*, 204–218.

[17] **Göksel, İ.**, **Antar, N. and Bakırtaş, İ.** (2015). Solitons of (1+1)D cubic-quintic nonlinear Schrödinger equation with $\mathcal{PT}$-symmetric potentials. *Optics Communications*, *354*, 277–285.

[18] **Bender, C.M. and Boettcher, S.** (1998). Real spectra in non-Hermitian Hamiltonians having $\mathcal{PT}$ symmetry. *Physical review letters*, *80*(24), 5243.

[19] **Yang, J.** (2014). Symmetry breaking of solitons in one-dimensional parity-time-symmetric optical potentials. *Optics letters*, *39*(19), 5547–5550.

[20] **Christodoulides, D. and Yang, J.** (2018). *Parity-time symmetry and its applications* (Vol. 280), Singapore: Springer.

[21] **Musslimani, Z.H.**, **Makris, K.G.**, **El-Ganainy, R. and Christodoulides, D.N.** (2008). Optical solitons in $\mathcal{PT}$ periodic potentials. *Physical Review Letters*, *100*(3), 030402.

[22] **Beekman, A.**, **Rademaker, L. and van Wezel, J.** (2019). An introduction to spontaneous symmetry breaking. *SciPost Physics Lecture Notes*, 011.

[23] **Alberucci, A.**, **Piccardi, A.**, **Kravets, N.**, **Buchnev, O. and Assanto, G.** (2015). Soliton enhancement of spontaneous symmetry breaking. *Optica*, *2*(9), 783–789.

[24] **Wadati, M.** (2008). Construction of parity-time symmetric potential through the soliton theory. *Journal of the Physical Society of Japan*, *77*(7), 074005.

[25] **Yang, J.** (2014). Can parity-time-symmetric potentials support families of non-parity-time-symmetric solitons?. *Studies in Applied Mathematics*, *132*(4), 332–353.

[26] **Russell, J.S.** (1844). Report on waves. *Report of the Fourteenth Meeting of the British Association for the Advancement of Science*, 311–390.

[27] **Korteweg, D.J. and De Vries, G.** (1895). XLI. On the change of form of long waves advancing in a rectangular canal, and on a new type of long stationary waves. *The London, Edinburgh, and Dublin Philosophical Magazine and Journal of Science*, *39*(240), 422–443.

[28] **Zabusky, N.J. and Kruskal, M.D.** (1965). Interaction of "solitons" in a collisionless plasma and the recurrence of initial states. *Physical review letters*, *15*(6), 240–243.

[29] **Ablowitz, M.J. and Segur, H.** (1981). *Solitons and the inverse scattering transform*. Society for Industrial and Applied Mathematics.

[30] **Benney, D.J. and Newell, A.C.** (1967). The propagation of nonlinear wave envelopes. *Journal of mathematics and Physics*, *46*(1-4), 133–139.

[31] **Zakharov, V.E.** (1968). Stability of periodic waves of finite amplitude on the surface of a deep fluid. *Journal of Applied Mechanics and Technical Physics*, *9*(2), 190–194.

[32] **Shabat, A. and Zakharov, V.** (1972). Exact theory of two-dimensional self-focusing and one-dimensional self-modulation of waves in nonlinear media. *Sov. Phys. JETP*, *34*(1), 62.

[33] **Buryak, A.V. and Akhmediev, N.N.** (1995). Stability criterion for stationary bound states of solitons with radiationless oscillating tails. *Physical Review E*, *51*(4), 3572.

[34] **Akhmediev, N.N. and Buryak, A.V.** (1995). Interactions of solitons with oscillating tails. *Optics communications*, *121*(4-6), 109–114.

[35] **Kelley, P.** (1965). Self-focusing of optical beams. *Physical Review Letters*, *15*(26), 1005.

[36] **Vlasov, S.N.**, **Petrishchev, V.A. and Talanov, V.I.** (1971). Averaged description of wave beams in linear and nonlinear media (the method of moments). *Radiophysics and Quantum Electronics*, *14*(9), 1062–1070.

[37] **Weinstein, M.I.** (1982). Nonlinear Schrödinger equations and sharp interpolation estimates. *Communications in Mathematical Physics*, *87*(4), 567–576.

[38] **Merle, F. and Raphael, P.** (2004). On universality of blow-up profile for L^2 critical nonlinear Schrödinger equation. *Inventiones mathematicae*, *156*(3), 565–672.

[39] **Moll, K.D.**, **Gaeta, A.L. and Fibich, G.** (2003). Self-similar optical wave collapse: observation of the Townes profile. *Physical review letters*, *90*(20), 203902.

[40] **Petviashvili, V.I.** (1976). Equation of an extraordinary soliton. *Fizika plazmy*, *2*, 469–472.

[41] **Ablowitz, M.J. and Biondini, G.** (1998). Multiscale pulse dynamics in communication systems with strong dispersion management. *Optics Letters*, *23*(21), 1668–1670.

[42] **Ablowitz, M.J. and Musslimani, Z.H.** (2001). Discrete diffraction managed spatial solitons. *Physical Review Letters*, *87*(25), 254102.

[43] **Ablowitz, M.J. and Musslimani, Z.H.** (2003). Discrete spatial solitons in a diffraction-managed nonlinear waveguide array: a unified approach. *Physica D: Nonlinear Phenomena*, *184*(1-4), 276–303.

[44] **Ablowitz, M.J. and Musslimani, Z.H.** (2003). Dark and gray strong dispersion-managed solitons. *Physical Review E*, *67*(2), 025601.

[45] **Musslimani, Z.H. and Yang, J.** (2004). Self-trapping of light in a two-dimensional photonic lattice. *JOSA B*, *21*(5), 973–981.

[46] **Ablowitz, M.J. and Musslimani, Z.H.** (2005). Spectral renormalization method for computing self-localized solutions to nonlinear systems. *Optics letters*, *30*(16), 2140–2142.

[47] **Yang, J. and Lakoba, T.I.** (2007). Universally-convergent squared-operator iteration methods for solitary waves in general nonlinear wave equations. *Studies in Applied Mathematics*, *118*(2), 153–197.

[48] **Gagnon, L.** (1989). Exact traveling-wave solutions for optical models based on the nonlinear cubic-quintic Schrödinger equation. *JOSA A*, *6*(9), 1477–1483.

[49] **Yang, J.** (2019). Symmetry breaking with opposite stability between bifurcated asymmetric solitons in parity-time-symmetric potentials. *Optics Letters*, *44*(11), 2641–2644.

[50] **Yang, J.** (2015). Symmetry breaking of solitons in two-dimensional complex potentials. *Physical Review E*, *91*(2), 023201.

[51] **Li, P.**, **Dai, C.**, **Li, R. and Gao, Y.** (2018). Symmetric and asymmetric solitons supported by a $\mathcal{PT}$-symmetric potential with saturable nonlinearity: bifurcation, stability and dynamics. *Optics Express*, *26*(6), 6949–6961.

[52] **He, X.**, **Ning, T.**, **Zheng, J.**, **Li, J.**, **Pei, L.**, **Bai, B. and You, H.** (2021). Suppression of symmetry breaking of nonlinear modes by defocusing saturable nonlinearity in parity-time symmetric potentials. *JOSA B*, *38*(8), 2290–2296.

[53] **Feng, B.F.**, **Kawahara, T.**, **Mitsui, T. and Chan, Y.S.** (2005). Solitary-wave propagation and interactions for a sixth-order generalized Boussinesq equation. *International Journal of Mathematics and Mathematical Sciences*, *2005*(9), 1435–1448.

[54] **Yang, J.** (2002). Internal oscillations and instability characteristics of (2+1)-dimensional solitons in a saturable nonlinear medium. *Physical Review E*, *66*(2), 026601.

[55] **Mitchell, M.**, **Segev, M.**, **Coskun, T.H. and Christodoulides, D.N.** (1997). Theory of self-trapped spatially incoherent light beams. *Physical Review Letters*, *79*(25), 4990.

[56] **Kevrekidis, P.G.**, **Rasmussen, K.O. and Bishop, A.R.** (2000). Localized excitations and their thresholds. *Physical Review E*, *61*(4), 4652.

[57] **Boyd, J.P.** (2001). *Chebyshev and Fourier Spectral Methods*. Courier Corporation.

[58] **Chen, M.** (2000). Solitary-wave and multi-pulsed traveling-wave solutions of Boussinesq systems. *Applicable Analysis*, *75*(1-2), 213–240.

[59] **Boyd, J.P.** (2007). Why Newton's method is hard for travelling waves: Small denominators, KAM theory, Arnold's linear Fourier problem, non-uniqueness, constraints and erratic failure. *Mathematics and Computers in Simulation*, *74*(2-3), 72–81.

[60] **Antar, N.** (2014). Pseudospectral renormalization method for solitons in quasicrystal lattice with the cubic-quintic nonlinearity. *Journal of Applied Mathematics*, *2014*.

[61] **Göksel, İ.**, **Antar, N. and Bakırtaş, İ.** (2018). Two-dimensional solitons in cubic-saturable media with $\mathcal{PT}$-symmetric lattices. *Chaos, Solitons & Fractals*, *109*, 83–89.

[62] **Yang, J. and Lakoba, T.I.** (2008). Accelerated imaginary-time evolution methods for the computation of solitary waves. *Studies in Applied Mathematics*, *120*(3), 265–292.

[63] **Epstein, C.L.** (2003). Mathematics of medical imaging.

[64] **Golub, G.H. and Van Loan, C.F.** (1996). *Matrix computations*. (Third edition), Johns Hopkins University Press.

[65] **Bender, C.M.**, **Hassanpour, N.**, **Hook, D.W.**, **Klevansky, S.P.**, **Sünderhauf, C. and Wen, Z.** (2017). Behavior of eigenvalues in a region of broken $\mathcal{PT}$ symmetry. *Physical Review A, , 95*(5), 052113.

[66] **Kreyszig, E.** (1991). *Introductory functional analysis with applications* (Vol. 17). John Wiley & Sons.

CURRICULUM VITAE

Name Surname **:** Melis TURGUT

EDUCATION

- **B.Sc. (Major)** **:** 2016, Mimar Sinan Fine Arts University, Faculty of Science and Letters, Department of Mathematics
- **B.Sc. (Minor)** **:** 2016, Mimar Sinan Fine Arts University, Faculty of Science and Letters, Actuary Programme
- **M.Sc.** **:** 2022, Istanbul Technical University, Graduate School, Department of Mathematics Engineering

PROFESSIONAL EXPERIENCE:

- March 2022 - Present: Research Assistant at Istanbul Technical University, Department of Mathematics Engineering

OTHER PUBLICATIONS, PRESENTATIONS AND PATENTS:

- **Bağcı, M., Turgut, M., Antar, N. and Bakırtaş, İ.** (2022). Dipole Solitons in a Nonlocal Nonlinear Medium with Self-Focusing and Self-Defocusing Quintic Nonlinear Responses. *Vortex Dynamics: From Physical to Mathematical Aspects*, IntechOpen.

- **Turgut, M. and Bakırtaş, İ.** (2021). Dördüncü Mertebeden Dispersiyon İçeren Kübik Nonlineer Schrödinger Denkleminin Çift-Kuyulu Bir Potansiyel Altında Soliton Çözümleri. *22. Ulusal Mekanik Kongresi*, 6–10 Eylül 2021, Adana, Türkiye.